Energetic, Structural, and Dynamic Aspects of Ethylene Polymerization Mediated by Homogeneous Single-Site "Constrained Geometry Catalysts" in the Presence of Cocatalyst and Solvation: An Investigation at the ab Initio Quantum Chemical Level

Giuseppe Lanza,*[,†] Ignazio L. Fragalà,*[,‡] and Tobin J. Marks*[,§]

Dipartimento di Chimica, Università della Basilicata, 85100, Potenza, Italy, Dipartimento di Scienze Chimiche, Università di Catania, 95125 Catania, Italy, and Department of Chemistry, Northwestern University, Evanston, Illinois 60208-3113

Received September 17, 2002

Mechanistic aspects of the ethylene insertion pathway into the Ti−methyl bond of the $[H_2Si(C_5H_4)(^tBuN)]TiCH_3^+H_3CB(C_6F_5)_3^-$ ion pair have been analyzed at the ab initio level, employing a double-ζ quality basis set and second-order perturbative Møller−Plesset (MP2) and by hybrid density functional B3LYP methods, including solvation effects and thermal and pressure corrections to 298 K/1.0 atm. Three basic reaction pathways are identified as viable. Ethylene approach from the side opposite the $H_3CB(C_6F_5)_3^-$ counteranion is energetically most favored and occurs in a concerted (intermediateless) fashion. The other two channels involving olefin approach on the same side as the $H_3CB(C_6F_5)_3^-$ group are energetically similar, and each occurs via two discrete steps: (i) anion displacement with formation of an intermediate π-ethylene complex, (ii) ethylene insertion into the Ti−C bond (the slow step). These latter pathways are more strongly solvent-assisted because of the larger attendant ion pair separation. Structural and energetic analysis of the $[H_2Si(C_5H_4)(^tBuN)]$-$Ti(n\text{-}C_3H_7)^+H_3CB(C_6F_5)_3^-$ insertion product shows the existence of several stable conformations. All such structures can be classified into two different types depending on the $[H_2Si(C_5H_4)(^tBuN)]Ti(n\text{-}C_3H_7)^+\cdots H_3CB(C_6F_5)_3^-$ contact distance. Structures with short $Ti^+\cdots[H_3CB(C_6F_5)_3]^-$ contacts involve metal coordinative saturation by the CH_3^- group or a counteranion aryl F. For structures with longer $Ti^+\cdots[H_3CB(C_6F_5)_3]^-$ contacts, the counteranion remains out of the metal coordination sphere and agostic interactions occur between the *n*-propyl chain and Ti. The relative stabilities of these classes of structures are an index of the preferred olefin enchainment mechanism: chain migratory insertion (dissociated ion pair) versus nonmigratory insertion (associated ion pair). Ethylene insertion into the Ti−$n\text{-}C_3H_7$ bond of the $[H_2Si(C_5H_4)(^tBuN)]Ti(n\text{-}C_3H_7)^+H_3CB(C_6F_5)_3^-$ ion pair occurs with a reduced overall energy barrier versus the corresponding methyl derivative, indicating that propagation should be more rapid than initiation. These results are discussed in the context of the large quantity of emerging experimental data.

Introduction

The past two decades have witnessed increasingly great interest in the insertive polymerization of olefins by early transition metal catalysts.[1] Group 4 constrained geometry catalysts (CGC; **I**) are particularly versatile

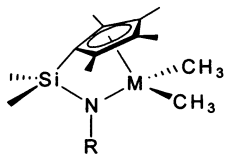

I

for polymerization and afford polyolefins with remarkable new architectural and processability characteristics.[2] A rich and varied class of catalysts has been obtained by variation of metal, cyclopentadienyl substituents (H, CH_3, indenyl, fluorenyl etc.), nitrogen substituents (CH_3, ^iPr, ^tBu, phenyl, etc.), and bridging

† Università della Basilicata.
‡ Università di Catania.
§ Northwestern University.

(1) For recent reviews, see: (a) Gladysz, J. A., Ed. *Chem. Rev.* **2000**, *100* (special issue on "Frontiers in Metal-Catalyzed Polymerization"). (b) Marks, T. J., Stevens, J. C., Eds. *Top. Catal.* **1999**, *7*, 1 (special volume on Advances in Polymerization Catalysis. Catalysts and Processes). (c) Scheirs J.; Kaminsky, W. *Metallocene-Based Polyolefins: Preparation, Properties, and Technology*; John Wiley & Sons: New York, 1999; Vols. 1 and 2. (d) Kaminsky, W. *Metalorganic Catalysts for Synthesis and Polymerization: Recent Results by Ziegler−Natta and Metallocene Investigations*; Springer-Verlag: Berlin, 1999. (e) Britovsek, G. J. P.; Gibson, V. C.; Wass, D. F. *Angew. Chem., Int. Ed.* **1999**, *38*, 428 (nonmetallocene olefin polymerization catalysts). (f) Jordan, R. F. *J. Mol. Catal.* **1998**, *128*, 1 (special issue on metallocene and single-site olefin catalysts). (g) McKnight, A. L.; Waymouth, R. M. *Chem. Rev.* **1998**, *98*, 2587 (constrained geometry polymerization catalysts). (h) Kaminsky, W.; Arndt, M. *Adv. Polym. Sci.* **1997**, *127*, 144. (i) Bochmann, M. *J. Chem. Soc., Dalton Trans.* **1996**, 255. (j) Brintzinger, H. H.; Fischer, D.; Mülhaupt, R.; Rieger, B.; Waymouth, R. M. *Angew. Chem., Int. Ed. Engl.* **1995**, *34*, 1143. (k) Soga, K.; Teramo, M. *Catalyst Design for Tailor-Made Polyolefins*; Elsevier: Amsterdam, 1994.

10.1021/om0207764 CCC: $22.00
Publication on Web 11/12/2002

group ($(CH_3)_2Si$, $(CH_3)_2C$, $(CH_2)_2$, etc).[2] CGC systems exhibit electronic and steric properties intermediate between those of *ansa*-metallocene (e.g., $(CH_3)_2Si(R_4C_5)_2MR^+$) and half-sandwich (e.g., $(R_4C_5)MR_2^+$) catalysts.[1−4] The formal electronic unsaturation and sterically accessible surface at the metal center increase in the order $[(CH_3)_2Si(R_4C_5)_2]MR^+ < [(CH_3)_2Si(R_4C_5)(^tBuN)]MR^+ < (R_5C_5)MR_2^+$.

The sterically encumbered active site in *ansa*-biscyclopentadienyl catalysts promotes the polymerization of ethylene and propylene, with very high stereocontrol possible in the latter case.[3] At the other extreme, half-sandwich complexes mediate the syndiospecific polymerization of sterically encumbered olefins such as styrenes.[4] Cyclopentadienyl-amido-based catalysts effect the homopolymerization of long-chain α-olefins (1-butene and 1-pentene) and ethylene, copolymerization with sterically encumbered comonomers, and, depending on the catalyst symmetry, moderately stereoselective enchainment, isotactic or syndiotatic, of propylene.[2,5]

The great advances in, and the development of, new catalytic processes are also intimately connected with the discovery of new *cocatalysts* capable of generating highly active and stable cationic systems.[6−8] Indeed, there is growing experimental evidence that cocatalyst-counterion "fit" and solvation play a significant role in the structures and energetics of the ion pairing, hence, catalytic activities and selectivities. Ion pairs are typically synthesized using neutral group 13 organo-Lewis acids such as methylalumoaxane (MAO),[6] BAr^F_3, and $AlAr^F_3$ reagents (Ar^F = fluoroaryl group)[7] or salt-like activators such as $Ph_3C^+X^-$, $HNR_3^+X^-$, and Fc^+X^- (X^- = $BAr^F{}_4^-$, $AlAr^F{}_4^-$, $M(OAr^F)_n^-$) reagents.[8] MAO, a mixture of rapidly equilibrating $(MeAlO)_n$-like cage/cluster species, is generally employed in great stoichiometric excess,[1,6] affords a weakly coordinating counteranion, scavenges impurities, and is thought to prevent bimolecular reductive H-transfer catalyst deactivation.[1,6] Nevertheless, MAO is expensive and the complex nature hampers unambiguous structural/dynamic characterization in solution, hence precludes rational control of catalyst properties. In contrast, recently developed borane[7] and borate[8] cocatalysts yield structurally well-defined cation−anion pairs with moderate to very high polymerization activities,[1,7,8] in some cases with higher productivies than MAO-activated systems,[2c] and in addition tolerate some classes of functionalized reagents.[9] The structurally well-defined nature of these catalysts also allows systematic studies of thermochemistry, metrical parameters, and solution structural dynamics, providing insight into the nature of cation−anion interactions as well as the kinetics and selectivity of olefin polymerization.[10−15] Moreover, systematic analysis of catalyst−cocatalyst architecture has yielded a considerable body of empirical structure−activity correlations.[10−15] Nevertheless, a detailed quantitative understanding of the relationship between active site ion pair structure and catalytic properties is far from realization.

(2) (a) Hair, G. S.; Jones, R. A.; Cowley, A. H.; Lynch, V. *Inorg. Chem.* **2001**, *40*, 1014. Chum, P. S.; Kruper, W.; Guest, M. J. *Adv. Mater.* **2000**, *12*, 1759. (c) Sinnema, P.-J.; Hessen, B.; Teuben, J. H. *Macromol. Rapid Commun.* **2000**, *21*, 562. (d) Leusen, D.; Beetstra, D. J.; Hessen, B.; Teuben, J. H. *Organometallics* **2000**, *19*, 4084. (e) Kleinschmidt, R.; Griebenow, Y.; Fink, G. *J. Mol. Catal. A: Chem.* **2000**, *157*, 83. (f) Brown, S. J.; Gao, X.; Harrison, D. G.; Koch, L.; Spence, R. E. H.; Yap, G. P. A. *Organometallics* **1998**, *17*, 5445. (g) Duda, L.; Erker, G.; Frohlich, R.; Zippel, F. *Eur. J. Inorg. Chem.* **1998**, 1153. (h) Chen, Y. X.; Marks, T. J. *Organometallics* **1997**, *16*, 3649. (i) Carpenetti, D. W.; Kloppenbrug, L.; Kupec, J. T.; Petersen, J. L. *Organometallics* **1996**, *15*, 1572. (j) Stevens, J. C. In *Studies in Surface Science and Catalysis*; Hightower, J. W., Delglass, W. N., Iglesia, E., Bell, A. T., Eds.; Elsevier: Amsterdam, 1996; Vol. 101, p 11. (k) Devore, D. D.; Timmers, F. J.; Hasha, D. L.; Rosen, R. K.; Marks, T. J.; Deck, P. A.; Stern, C. L. *Organometallics* **1995**, *14*, 3132. (l) Stevens, J. C. In *Catalyst Design for Tailor-Made Polyolefins*; Soga, K., Teramo, M., Eds.; Elsevier: Amsterdam, The Netherlands, 1994; p 277. (m) Stevens, J. C.; Timmers, F. J.; Wilson, D. R.; Schmidt, G. F.; Nickias, P. N.; Rosen, R. K.; Knight, G. W.; Lai, S. European Patent Application EP-416-815-A2, March 13, 1991. (n) Canich, J. A. PCT Application WO 91/04257, April, 4, 1991. (o) Okuda, J. *Chem. Ber.* **1990**, *123*, 1649. (p) Shapiro, P. J.; Bunel, E.; Schaefer, W. P.; Bercaw, J. E. *Organometallics* **1990**, *9*, 867.

(3) (a) Resconi, L.; Cavallo, L.; Fait, L.; Fait, A.; Piemontesi, F. *Chem. Rev.* **2000**, *100*, 1253. (b) Kaminsky, W. *J. Chem. Soc., Dalton Trans.* **1998**, 1413. (c) Möhring, P. C.; Coville, N. J. *J. Organomet. Chem.* **1994**, *479*, 1.

(4) (a) Yakota, Y.; Inoue, T.; Nagamura, S.; Shozaki, H.; Tomotsu, N.; Kuramoto, M.; Ishihara, N. In *Metalorganic Catalysts for Synthesis and Polymerization: Recent Results by Ziegler−Natta and Metallocene Investigations*; Kaminsky, W., Ed.; Springer-Verlag: Berlin, 1999; p 435. (b) Ewart, S. W.; Sarsfield, M. J.; Jeremic, D.; Tremblay, T. L.; Williams, E. F. F.; Baird, M. C. *Organometallics* **1998**, *17*, 1502. (c) Wang, Q.; Quyoum, R.; Gillis, D. J.; Tudoret, M.-J.; Jeremic, D.; Hunter, B. K.; Baird, M. C. *Organometallics* **1996**, *15*, 693. (d) Pellecchia, C.; Pappalardo, D.; Oliva, L.; Zambelli, A. *J. Am. Chem. Soc.* **1995**, *117*, 6593.

(5) (a) Shaffer, T. D.; Canich, J. A. M.; Squire, K. R. *Macromolecules* **1998**, *31*, 5145. (b) Hagihara, H.; Shiono, T.; Ikeda, T. *Macromolecules* **1998**, *31*, 3184. (c) Hagihara, H.; Shiono, T.; Ikeda, T. *Macromolecules* **1997**, *30*, 4783. (d) McKnight, A. L.; Masood, M. A.; Waymouth, R. M.; Straus, D. A. *Organometallics* **1997**, *16*, 2879. (e) Shiomura, T.; Asanuma, T.; Sunaga, T. *Macromol. Rapid. Commun.* **1997**, *18*, 169. (f) Shiomura, T.; Asanuma, T.; Inoue, N. *Macromol. Rapid Commun.* **1996**, *17*, 9.

(6) (a) Coevoet, D.; Cramail, H.; Deffieux, A. *Macromol. Chem. Phys.* **1998**, *199*, 1459. (b) Reddy, S. S.; Sivaram, S. *Prog. Polym. Sci.* **1995**, *20*, 309. (c) Harlan, C. J.; Bott, S. G.; Barron, A. R. *J. Am. Chem. Soc.* **1995**, *117*, 6465. (d) Sishta, C.; Harthorn, R.; Marks, T. J. *J. Am. Chem. Soc.* **1992**, *114*, 1112. (e) Pasynkiewicz, S. *Polyhedron* **1990**, *9*, 429.

(7) (a) Metz, M. V.; Schwartz, D. J.; Stern, C. L.; Marks, T. J.; Nickias, P. N. *Organometallics* **2002**, *21*, 4159. (b) Chen, Y.-X.; Kruper, W. J.; Roof, G.; Wilson, D. R. *J. Am. Chem. Soc.* **2001**, *123*, 745. (c) Zhou, J.; Lancaster, S. J.; Walter, D. A.; Beck, S.; Thornton-Pett, M.; Bochmann, M. *J. Am. Chem. Soc.* **2001**, *123*, 223. (d) Chase, P. A.; Piers, W. E.; Patrick, B. O. *J. Am. Chem. Soc.* **2000**, *122*, 12911. (e) Li, L.; Stern, C. L.; Marks, T. J. *Organometallics* **2000**, *19*, 3332. (f) Luo, L.; Marks, T. J. *Top. Catal.* **1999**, *15*, 97. (g) Li, L.; Marks, T. J. *Organometallics* **1998**, *17*, 3996. (h) Deck, P. A.; Beswick, C. L.; Marks, T. J. *J. Am. Chem. Soc.* **1998**, *120*, 1772. (i) Piers, W. E.; Chivers, T. *Chem. Soc. Rev.* **1997**, *26*, 345. (j) Yang, X.; Stern, C. L.; Marks, T. J. *J. Am. Chem. Soc.* **1994**, *116*, 10015. (k) Bochmann, M.; Lancaster, S. J.; Hursthous, M. B.; Malik, K. M. *Organometallics* **1994**, *13*, 2235. (l) Yang, X. M.; Stern, C. L.; Marks, T. J. *J. Am. Chem. Soc.* **1991**, *113*, 3623.

(8) (a) Metz, M. V.; Sun, Y.; Stern, C. L.; Marks, T. J. *Organometallics* **2002**, *21*, 369. (b) Chen, M.-C.; Marks, T. J. *J. Am. Chem. Soc.* **2001**, *123*, 11803. (c) Sun, Y. M.; Metz, M. V.; Stern, C. L.; Marks, T. J. *Organometallics* **2000**, *19*, 1625. (d) Metz, M. V.; Schwartz, D. J.; Stern, C. L.; Nickias, P. N.; Marks, T. J. *Angew. Chem., Int. Ed.* **2000**, *39*, 1312. (e) Chen, Y.-X.; Stern, C. L.; Marks, T. J. *J. Am. Chem.* **1997**, *119*, 2582. (f) Jia, L.; Yang, X.; Stern, C. L.; Marks, T. J. *Organometallics* **1997**, *16*, 842. (g) Chien, J. C. W.; Tsai, W.-M.; Rausch, M. D. *J. Am. Chem. Soc.* **1991**, *113*, 8570. (h) Yang, X.; Stern, C. L.; Marks, T. J. *Organometallics* **1991**, *10*, 840. (i) Ewen, J. A.; Elder, M. J.; Ewen, J. A.; Elden, M. J. European Patent Appl. p 426637, 1991. (j) Hlatky, G. G.; Upton, D. J.; Turner, H. W. U.S. Patent Appl. p 459921, 1990.

(9) (a) Xu, G.; Chung, T. C. *Macromolecules* **2000**, *33*, 5803. (b) Xu, G.; Chung, T. C. *Macromolecules* **1999**, *32*, 8689. (c) Xu, G.; Chung, T. C. *J. Am. Chem. Soc.* **1999**, *121*, 6763. (d) Chung, T. C.; Janvikul, W. *J. Organomet. Chem.* **1999**, *581*, 176. (e) Koo, K.; Marks, T. J. *J. Am. Chem. Soc.* **1998**, *120*, 4019. (f) Collins, S.; Ward, D. G. *Macromolecules* **1995**, *27*, 7222. (g) Deng, H.; Shiono, T.; Soga, K. *Macromolecules* **1995**, *27*, 3067. (h) Collins, S.; Ward, D. G. *J. Am. Chem. Soc.* **1992**, *114*, 5460.

(10) (a) Erker, G. *Acc. Chem. Res.* **2001**, *34*, 309. (b) Dahlmann, M.; Erker, G.; Bergander, K. *J. Am. Chem. Soc.* **2000**, *122*, 7986. (c) Dahlmann, M.; Erker, G.; Nissien, M.; Fröhlich, R. *J. Am. Chem. Soc.* **1999**, *121*, 2820. (d) Karl, J.; Dahlmann, M.; Erker, G.; Bergander, K. *J. Am. Chem. Soc.* **1998**, *120*, 5643. (e) Temme, B.; Erker, G.; Karl, J. Luftmann, H.; Fröhlich, R.; Kotila, S. *Angew. Chem., Int. Ed. Engl.* **1995**, *34*, 1755.

In this context, theoretical studies can play a central role in providing information complementary to experiment on the nature of the true catalytic species and the interplay between catalyst−cocatalyst architecture and polymerization activity and selectivity.[16−27] Early studies focused exclusively on qualitative understanding of the basic polymerization mechanisms for "naked" catalyst cations.[16−21] Analysis of a homologous series of model complexes affords valuable qualitative rationales for the kinetics and varying catalytic activities as a function of ligand, metal, and olefin. However, more in-depth investigations are required to obtain crucial quantitative information on reaction coordinates involving what we now know to be the true catalytic species: *cation−anion−olefin−solvent ensembles*. Indeed, there are now increasing efforts to analyze counteranion and solvent effects in olefin polymerization catalysis. Fusco et al.[22] carried out density functional theory (DFT) studies on heterolytic ion pair separation energetics and ethylene insertion into $(C_5H_5)_2MCH_3^+X^-$ (M = Ti, Zr; $X^- = Al(CH_3)_2Cl_2^-$, $Al(CH_3)_3Cl^-$, $Cl_2Al[O(Al(CH_3)_3)AlH(CH_3)]_2^-$) systems without considering solvent effects. Bernardi et al.[24b] performed DFT calculations on the $Cl_2TiCH_3^+Cl_2AlH_2^-$ model ion pair including solvent effects. Klesing et al.[24a] estimated the competitive stabilization of cationic *ansa*-bis-indenyl sites by propylene, neutral Zr dialkyls, and hexameric MAO-like anion clusters. Nifant'ev et al.[25] reported DFT studies on the energetics associated with ethylene insertion into $(C_5H_5)_2ZrC_2H_5^+X^-$ ion pairs ($X^- = H_3CB(C_6F_5)_3^-$, $B(C_6F_5)_4^-$) explicitly including entropic contributions, but ignoring solvation and Zr relativistic effects. Ziegler et al.[26] reported DFT studies on aspects of catalyst generation in half-sandwich, CGC, and metallocene systems with various boron- and aluminum-based cocatalysts and also analyzed ethylene coordination/insertion at $(C_5H_5)_2ZrC_2H_5^+H_3CB(C_6F_5)_3^-$ and $(C_5H_5)_2ZrC_2H_5^+B(C_6F_5)_4^-$ contact ion pairs.

In previous work, we reported the first ab initio computational examination, including counteranion, solvation, and ligand substituent effects, on *catalyst*

(11) (a) Carpentier, J.-F.; Maryin, V. P.; Luci, J.; Jordan, R. F. *J. Am. Chem. Soc.* **2001**, *123*, 898. (b) Carpentier, J.-F.; Wu, Z.; Lee, W. C.; Strömberg, S.; Christopher, J. N.; Jordan, R. F. *J. Am. Chem. Soc.*, **2000**, *122*, 7750. (c) Casey, C. P.; Carpenetti, D. W., II. *Organometallics* **2000**, *20*, 3970. (d) Casey, C. P.; Carpenetti, D. W., II; Sakurai, H. *J. Am. Chem. Soc.* **1999**, *121*, 9483. (e) Abrams, M. B.; Yoder, J. C.; Loeber, C.; Day, M. V.; Bercaw, J. E. *Organometallics* **1999**, *18*, 1389. (f) Galakhov, M. V.; Heinz, G.; Royo, P. *Chem. Commun.* **1998**, 17. (g) Casey, C. P.; Fagan, M. A.; Hallenbeck, S. L. *Organometallics* **1998**, *17*, 287. (h) Casey, C. P.; Hallenbeck, S. L.; Wright, J. M.; Landis, C. R. *J. Am. Chem. Soc.* **1997**, *119*, 9680. (i) Temme, B.; Karl, J.; Erker, G. *Chem. Eur. J.* **1996**, *2*, 919. (j) Casey, C. P.; Hallenbeck, S. L.; Pollock, D. W.; Landis, C. R. *J. Am. Chem. Soc.* **1995**, *117*, 9770. (k) Wu, Z.; Jordan, R. F. *J. Am. Chem. Soc.* **1995**, *117*, 5867.

(12) (a) Beck, S.; Lieber, S.; Schaper, F.; Geyer, A.; Brintzinger, H.-H. *J. Am. Chem. Soc.* **2001**, *123*, 1483. (b) Beck, S.; Prosenc, M.-H.; Brintzinger, H.-H. *J. Mol. Catal. A: Chem.* **1998**, *128*, 41.

(13) (a) Beswick, C. L.; Marks, T. J. *J. Am. Chem. Soc.* **2000**, *122*, 10358. (b) Chen, Y.-X.; Marks, T. J. *Chem. Rev.* **2000**, *100*, 1391. (c) Beswick, C. L.; Marks, T. J. *Organometallics* **1999**, *18*, 2410. (d) Chen, Y.-X.; Metz, M. V.; Li, L.; Stern, C. L.; Marks, T. J. *J. Am. Chem.* **1998**, *120*, 6287. (e) Deck, P. A.; Beswick, C. L.; Marks, T. J. *J. Am. Chem. Soc.* **1998**, *120*, 1772. (f) Chen, Y.-X.; Stern, C. L.; Yang, S. T.; Marks, T. J. *J. Am. Chem. Soc.* **1996**, *118*, 12451. (g) Giardello, M. A. Eisen, M. S. Stern, C. L. Marks T. J. *J. Am. Chem. Soc.* **1995**, *117*, 12114. (h) Deck, P. A.; Marks, T. J. *J. Am. Chem. Soc.* **1995**, *117*, 6128.

(14) (a) Liu, Z.; Somsook, E.; White, C. B.; Rosaaen, K. A.; Landis, C. R. *J. Am. Chem. Soc.* **2001**, *123*, 11193. (b) Beck, S.; Brintzinger, H.-H.; Suhm, J.; Mülhaupt, R. *Macromol. Rapid Commun.* **1998**, *19*, 235. (c) Eisch, J. J.; Pombrik, S. I.; Gurtzgen, S.; Rieger, R., Huzier, W. In *Catalyst Design for Tailor-Made Polyolefins*; Soga, K., Teramo, M., Eds.; Elsevier: Amsterdam, The Netherlands, 1994; p 221.

(15) (a) Feichtinger, D.; Plattner, D. A.; Chen, P. *J. Am. Chem. Soc.* **1998**, *120*, 7125. (b) Richardson, D. E.; Alameddin, N. G.; Ryan, M. F.; Hayes, T.; Eyler, J. R.; Siedle, A. R. *J. Am. Chem. Soc.* **1996**, *118*, 11244. (c) Alameddin, N. G.; Ryan, M. F.; Eyler, J. R.; Siedle, A. R.; Richardson, D. E. *Organometallics* **1995**, *14*, 5005.

(16) (a) Vyboishchikov, S. F.; Musaev, D. G.; Froese, R. D. J.; Morokuma, K. *Organometallics* **2001**, *20*, 309. (b) Froese, R. D. J.; Musaev, D. G.; Morokuma, K. *Organometallics* **1999**, *18*, 373. (c) Das, P. K.; Dockter, D. W.; Fahey, D. R.; Lauffer, D. E.; Hawkins, G. D.; Li, J.; Zhu, T.; Cremer, C. J.; Truhlar, D. G.; Dapprich, S.; Froese, R. D. J.; Holtahusen, M. C.; Liu, Z.; Mogi, S.; Vibroschchikov, S.; Musaev, D. G.; Morokuma, K. In *Transition State Modeling for Catalysis*; Truhlar, D. G., Morokuma, K., Eds.; ACS Series; Washington, DC, 1999. (d) Froese, R. D. J.; Musaev, D. G.; Morokuma, K. *J. Mol. Struct. (THEOCHEM)* **1999**, *461−462*, 121. (e) Yoshida, T.; Koga, N.; Morokuma, K. *Organometallics* **1996**, *15*, 766. (f) Yoshida, T.; Koga, N.; Morokuma, K. *Organometallics* **1995**, *14*, 746. (g) Kawamura-Kuribayashi, H.; Koga, N.; Morokuma, K. *J. Am. Chem. Soc.* **1992**, *114*, 8687. (h) Kawamura-Kuribayashi, H.; Koga, N.; Morokuma, K. *J. Am. Chem. Soc.* **1992**, *114*, 2359.

(17) (a) Weiss, H.; Ehrig, M.; Ahlrichs, R. *J. Am. Chem. Soc.* **1994**, *116*, 4919. (b) Bierwagen, E. P.; Bercaw, J. E.; Goddard, W. A., III. *J. Am. Chem. Soc.* **1994**, *116*, 1481. (c) Jolly, C. A.; Marynick, D. S. *J. Am. Chem. Soc.* **1989**, *111*, 7968.

(18) (a) Margl, P. M.; Deng, L.; Ziegler, T. *J. Am. Chem. Soc.* **1999**, *121*, 154. (b) Margl, P. M.; Deng, L.; Ziegler, T. *Top. Catal.* **1999**, *7*, 187. (c) Margl, P. M.; Deng, L.; Ziegler, T. *Organometallics* **1998**, *17*, 933. (d) Margl, P. M.; Deng, L.; Ziegler, T. *J. Am. Chem. Soc.* **1998**, *120*, 5517. (e) Margl, P. M.; Woo, T. K.; Blöchl, P. E.; Ziegler, T. *J. Am. Chem. Soc.* **1998**, *120*, 2174. (f) Woo, T. K.; Margl, P. M.; Ziegler, T.; Blöchl, P. E. *Organometallics* **1997**, *16*, 3454. (g) Woo, T. K.; Margl, P. M.; Lohrenz, J. C. W.; Blöchl, P. E.; Ziegler, T. *J. Am. Chem. Soc.* **1996**, *118*, 13021. (h) Margl, P. M.; Lohrenz, J. C. W.; Ziegler, T.; Blöchl, P. E. *J. Am. Chem. Soc.* **1996**, *118*, 4434. (i) Lohrenz, J. C. W.; Woo, T. K.; Ziegler, T. *J. Am. Chem. Soc.*, **1995**, *117*, 12793. (j) Fan, L.; Harrison, D.; Woo, T. K.; Ziegler, T. *Organometallics* **1995**, *14*, 2018. (k) Woo, T. K.; Fan, L.; Ziegler, T. *Organometallics* **1994**, *13*, 2252. (l) Woo, T. K.; Fan, L.; Ziegler, T. *Organometallics* **1994**, *13*, 432.

(19) (a) Thorshaug, K.; Stovneng, J. A.; Rytter, E. *Macromolecules* **2000**, *33*, 8136. (b) Thorshaug, K.; Stovneng, J. A.; Rytter, E.; Ystenes, M. *Macromolecules* **1998**, *31*, 7149. (c) Stovneng, J. A.; Rytter, E. *J. Organomet. Chem.* **1996**, *519*, 277. (d) Doremaele, G. H. J. V.; Meier, R. J.; Iarlori, S.; Buda, F. *J. Mol. Struct. (THEOCHEM)* **1996**, *363*, 269. (e) Iarlori, S.; Buda, F.; Meier, R. J.; Doremaele, G. H. J. V. *Mol. Phys.* **1996**, *87*, 801. (f) Meier, R. J.; Doremaele, G. H. J. V.; Iarlori, S.; Buda, F. *J. Am. Chem. Soc.* **1994**, *116*, 7274.

(20) (a) Lieber, S.; Prosenc, M.-H.; Brintzinger, H.-H. *Organometallics* **2000**, *19*, 377. (b) Prosenc, M.-H.; Schaper, F.; Brintzinger, H.-H. N. In *Metalorganic Catalysts for Synthesis and Polymerization: Recent Results by Ziegler−Natta and Metallocene Investigations*; Kaminsky, W., Ed.; Springer-Verlag: Berlin, Germany, 1999; p 223. (c) Prosenc, M.-H.; Brintzinger, H.-H. *Organometallics* **1997**, *16*, 3889. (d) Prosenc, M.-H.; Janiak, C.; Brintzinger, H.-H. *Organometallics* **1992**, *11*, 4036.

(21) (a) Peluso, A.; Improta, R.; Zambelli, A. *Organometallics* **2000**, *19*, 411. (b) Improta, R.; Garzillo, C.; Peluso, A. *J. Mol. Struct. (THEOCHEM)* **1998**, *426*, 249. (c) Peluso, A.; Improta, R.; Zambelli, A. *Macromolecules* **1997**, *30*, 2219. (d) Guerra, G.; Cavallo, L.; Corradini, P.; Fusco, R. *Macromolecules* **1997**, *30*, 677.

(22) (a) Fusco, R.; Longo, L.; Proto, A.; Masi, F.; Garbasi, F. *Macromol. Rapid Commun.* **1998**, *19*, 257. (b) Fusco, R.; Longo, L.; Masi, F.; Garbasi, F. *Macromol.* **1997**, *30*, 7673. (c) Fusco, R.; Longo, L.; Masi, F.; Garbasi, F. *Macromol. Rapid Commun.* **1997**, *18*, 433.

(23) (a) Lanza, G.; Fragalà, I. L.; Marks, T. J. *Organometallics* **2001**, *20*, 4006. (b) Lanza, G.; Fragalà, I. L.; Marks, T. J. *J. Am. Chem. Soc.* **2000**, *122*, 12764. (c) Lanza, G.; Fragalà, I. L. *Top. Catal.* **1999**, *15*, 45. (d) Lanza, G.; Fragalà, I. L.; Marks, T. J. *J. Am. Chem. Soc.* **1998**, *120*, 8257.

(24) (a) Klesing, A.; Bettonville, S. *Chem. Phys. Phys. Chem.* **1999**, *1*, 2373. (b) Bernardi, F.; Bottoni, A.; Miscione, G. P. *Organometallics* **1998**, *17*, 16. (c) Jensen, V. R.; Børve, K. J.; Ystenes, M. *J. Am. Chem. Soc.* **1995**, *117*, 4109.

(25) (a) Nifant'ev, I. E.; Ustynyuk, L. Y.; Laikov, D. N. *Organometallics* ***2001***, *20*, *5375*. (b) Nifant'ev, I. E.; Ustynyuk, L. Y.; Laikov, D. N. *Russ. Chem. Bull. Int. Ed.* **2000**, *49*, 1164.

(26) (a) Vanka, K.; Ziegler, T. *Organometallics* **2001**, *20*, 905. (b) Chan, M. S. W.; Ziegler, T. *Organometallics* **2000**, *19*, 5182. (c) Vanka, K.; Chan, M. S. W.; Pye, C.; Ziegler, T. *Organometallics* **2000**, *19*, 1841. (d) Chan, M. S. W.; Vanka, K.; Pye, C. C.; Ziegler, T. *Organometallics* **1999**, *18*, 4624.

(27) (a) Moscardi, G.; Resconi, L.; Cavallo L. *Organometallics* **2001**, *20*, 1918. (b) Moscardi, G.; Piemontesi, F.; Resconi, L. *Organometallics* **1999**, *18*, 5264. (c) Guerra, G.; Longo P.; Corradini, P.; Cavallo, L. *J. Am. Chem. Soc.* **1999**, *121* (1), 8651. (d) Cavallo, L. Guerra, G.; Corradini, P. *J. Am. Chem. Soc.* **1998**, *120*, 2428. (e) Guerra, G.; Longo P.; Cavallo, L.; Moscardi, G.; Vacatello, M.; Corradini, P. *Macromolecules* **1996**, *29*, 4834.

generation and catalyst−cocatalyst structural energetics for a CGCTi(CH_3)$_2$-based precatalyst activated with B(C_6F_5)$_3$.[23] One early study[23d] communicated preliminary results on energetic profiles for olefin activation/insertion at the [$H_2Si(C_5H_4)(^tBuN)$]Ti$CH_3^+H_3CB(C_6F_5)_3^-$ ion pair, including solvation. It was suggested on the basis of the limited data at hand that counteranion and solvent cannot be ignored. In the intervening period, considerably more experimental data on the role of ion pair structure, dynamics, and solvation in the olefin enchainment process have become available.[7,8,13] Here we now report a full account of our theoretical analyses at the ab initio SCF MP2 and DFT-B3LYP levels, focusing on reaction pathways for ethylene insertion at $H_2Si(C_5H_4)(^tBuN)TiR^+H_3CB(C_6F_5)_3^-$ (R = CH_3 and *n*-C_3H_7) ion pairs, including solvation and entropic effects, and compare our results with experiment. The new issues we address here as a function of these variables are (1) energetics of the catalyst−cocatalyst ion pairing and the importance of electrostatic interactions, (2) reaction coordinates for the various competing olefin approach/activation/enchainment pathways as a function of ion pairing strength, (3) stability and mobility of Ti-alkyl$^+$ structures as a function of ion pairing strength, (4) detailed analysis of olefin complexation and insertion energetics as a function of ion pairing strength and comparison with recent experimental data, (5) one-on-one comparison of olefin approach/activation/enchainment pathways for the same catalyst with and without the counteranion to allow analysis of ion pairing effects, (6) effects of a Ti-polymer chain on the insertive transition state and ion pairing strength, (7) comparison of HF and DFT-B3LYP derived geometries in order to assess the role of electron correlation for systems with weak bonding interactions, (8) analysis of entropic contributions to the observed reaction energetics.

Computational Details

The effective core potentials (ECP) of Hay and Wadt,[28] which explicitly treat semicore s and p electrons and a basis set contracted as [541/511/41], were used for Ti. The standard all-electron 6-31G basis was used for the remaining atoms.[29] Geometry optimization used analytical gradient techniques within the restricted Hartree−Fock (HF) formalism, and the threshold adopted for convergence was 0.0004 hartree/bohr on the gradient. No local symmetry and no geometrical constraints were imposed in optimization.

The "distinguished reaction coordinate procedure" was used in analysis of the transition state geometry for ethylene insertion, and the reaction coordinate was associated with the vector along the emerging C−C σ bond ($TiCH_3\cdots CH_2{=}CH_2$). However, in the case of pathway C (vide infra), this reaction coordinate is not well-suited, and the vector along the emerging Ti−C σ bond ($CH_3Ti\cdots CH_2{=}CH_2$) was adopted instead. For each pathway, the geometry optimization of the first point (longest C−C or Ti−C distance) was begun from the ground state structure of the [$H_2Si(C_5H_4)(^tBuN)$]Ti$(CH_3)^+H_3CB(C_6F_5)_3^-$ contact ion pair. As the reaction proceeded, the starting structure in each geometry optimization was taken from the immediately preceding point. Convergence of the geometry optimization procedures in the present systems proved particularly difficult because the $H_3CB(C_6F_5)_3^-$ group undergoes large displacements from equilibrium upon ethylene approach, and a large number of energy and gradient cycles was required to reach the desired threshold. An average of ~500 cycles was necessary for various points along reaction coordinates. This behavior reflects the unusual characteristics of the [$H_2Si(C_5H_4)(^tBuN)$]Ti$CH_3^+\cdots H_3CB(C_6F_5)_3^-$ interaction—largely isotropic and involving a very flat potential energy surface associated with anion excursions. There are, therefore, a large number of conformers very close in energy, depending on the $H_3CB(C_6F_5)_3^-$ group orientation. This feature strongly affected the computational execution (an average of 20 days on an IBM SP 8 parallel processor facility for each point on the reaction coordinate). The very slow convergence in geometry optimization is responsible for minor deviations of the present energy barriers and transition state geometries from those discussed in an earlier study of pathway A.[23d] In that case, a higher convergence cutoff was adopted in geometry optimization. Because the $H_3CB(C_6F_5)_3^-$ counteranion can assume numerous orientations with respect to the $H_2Si(C_5H_4)(^tBuN)TiCH_3^+$ framework (essentially a "rolling ball"), the position of borate in the final optimized structure can depend on the starting geometry (vide infra; the two different intermediate π-ethylene complexes along pathways B and C). However, the stationary points presently characterized by vibrational analysis are true minima or true transition states (no imaginary frequency and only one imaginary frequency, respectively).

Correlation effects were evaluated using a second-order perturbative treatment (MP2) where all valence electrons, including the semicore metal s and p, are correlated. For selected cases, computed energies (ΔE) were corrected for thermal and zero-point vibrational energies ($\Delta H°_{298}$) and entropies (ΔS) to obtain free energy changes ($\Delta G°_{298}$) at 298 K. The accuracy of the presently adopted level of theory, namely, HF geometry optimization, double-ζ basis function, and MP2 correlation treatment (DZV/MP2/HF), has been widely tested in a series of earlier studies on similar problems.[23] We have previously shown that such results compare favorably with those from both larger basis sets and coupled cluster single double excitation results,[23a] as well as with experimental data where available.[23b] In particular, using an extended basis set (all electrons on Ti and polarization functions on all atoms) and performing geometry optimizations at the MP2 level, the ethylene insertion energy barrier into the $H_2Si(C_5H_4)(^tBuN)TiCH_3^+$ naked cation is reduced only slightly with respect to that computed using the DZV/MP2/HF approach.[23a] However, high-order correlation effects up to the MP4-SDQ and CCSD levels were found to increase the energy barrier slightly.[23a] At the highest level of theory, DZP/MP4-SDQ/MP2, the computed insertion energy barrier of 7.5 kcal/mol is close to that evaluated with the DZV/MP2/RHF approach, 7.9 kcal/mol. Analogously, a previous study[23c] on the structure of the simpler $H_2Si(C_5H_4)(CH_3N)TiCH_3{\cdot}CH_3BF_3$ model contact ion pair analyzed both at HF and MP2 levels showed that equilibrium geometries are influenced by correlation in only a minor way and that small variations in bond distances are observed (<0.06 Å). Importantly, the ion pair strengths (energetics of ion pair formation from neutral precursors and heterolytic ion pair separation) are virtually identical using HF and MP2 optimized geometries. Therefore, the present DZV/MP2/RHF level of theory is a realistic compromise in terms of cost versus benefit, and the present data can be considered correct at a semiquantitative level. Nevertheless, we also performed alternative calculations employing nonlocal DFT methods with the exact reaction coordinate at the [$H_2Si(C_5H_4)(^tBuN)$]Ti$CH_3^+H_3CB(C_6F_5)_3^-$ ion pair.

Solvent effects were modeled using the self-consistent isodensity polarized continuum formalism (SCI-PCM). The SCI-PCM method models the solvent as a continuum of uniform dielectric constant, and the solute is placed into a cavity within the solvent. The cavity defined as an isodensity

(28) (a) Hay, P. J.; Wadt, W. R. *J. Chem. Phys.* **1985**, *82*, 299. (b) Hay, P. J.; Wadt, W. R. *J. Chem. Phys.* **1985**, *82*, 270.

(29) (a) Hehre, W. J.; Ditchfield, R.; Pople, J. A. *J. Chem. Phys.* **1972**, *56*, 2257. (b) Franel, M. M.; Pietro, W. J.; Hehre, W. J.; Binkley, J. S.; Gordon, M. S.; DeFrees, D. J.; Pople, J. A. *J. Chem. Phys.* **1982**, *77*, 3654.

surface of the molecule is determined self-consistently in the presence of the polarizable medium and is coupled with the electron density of the solute. In this approach, the effects of solvation are folded into the iterative SCF procedure.[30] The dielectric constants of the solvents investigated are C_6H_6, 2.274; C_6H_5Cl, 5.71; CH_2Cl_2, 9.08. All the calculations were performed using the G94 code[31] on IBM-SP and Origin 2000 systems.

Results

Energetics and Dynamics of Ion Pair Separation. The computed ground state arrangement of the $[H_2Si(C_5H_4)(^tBuN)]TiCH_3^+H_3CB(C_6F_5)_3^-$ catalyst−cocatalyst ion pair has a pseudotetrahedral geometry around the Ti center with the $H_3CB(C_6F_5)_3^-$ group bonded in a μ-CH_3 fashion, in good agreement with diffraction data.[23b] Several structures having aryl fluorine coordination to Ti are, however, energetically accessible within ~5 kcal/mol.[23b] It was previously shown that the $Ti^+\cdots H_3CB(C_6F_5)_3^-$ interaction is predominantly electrostatic in character and can be described by a rather flat potential surface along the Ti···C−B elongation vector.[23b] Moreover, Coulombic attractions depend inversely upon the dielectric constant of the medium, $E = q^+q^-/4\pi\epsilon r$, and therefore, solvation reduces the attraction binding the ion pair, thus rendering the potential energy surface along the $Ti^+\cdots H_3CB(C_6F_5)_3^-$ coordinate even flatter. This observation provides a suitable rationale for the stereochemical mobility of the $H_3CB(C_6F_5)_3^-$ group observed in dynamic NMR experiments and the solvent dependence thereof.[7h,13a,c,g] Figure 1A shows the computed potential energy surface for the $[H_2Si(C_5H_4)(^tBuN)]TiCH_3^+H_3CB(C_6F_5)_3^-$ structure along the displacement coordinate for heterolytic ion pair dissociation in the gas phase and in solution as a function of solvent dielectric constant.[32] In Figure 1B, potential energetic profiles, evaluated at the MP2 level for heterolytic separation in the gas phase and in benzene solution, are compared to those evaluated by the simple $E_{COUL} = q^+q^-/4\pi\epsilon r$ relationship, where q^+ and q^- are the computed Mulliken charges on the $H_2Si(C_5H_4)(^tBuN)TiCH_3^+$ and $H_3CB(C_6F_5)_3^-$ groups, r is the distance between the Ti and the $H_3CB(C_6F_5)_3^-$ geometrical centroid, and ϵ is the medium dielectric constant ($\epsilon = 1$ in the gas phase, 2.274 in benzene). It is evident that for $Ti^+\cdots[H_3CB(C_6F_5)_3]^-_{centr}$ distances greater than 6 Å, E_{MP2} and E_{COUL} in both the gas phase and benzene conform closely to hyperbolic behavior, a clear indication that $[H_2Si(C_5H_4)(^tBuN)]TiCH_3^+\cdots H_3CB(C_6F_5)_3^-$ interactions resemble those describable by isotropic Coulombic attractions with charges

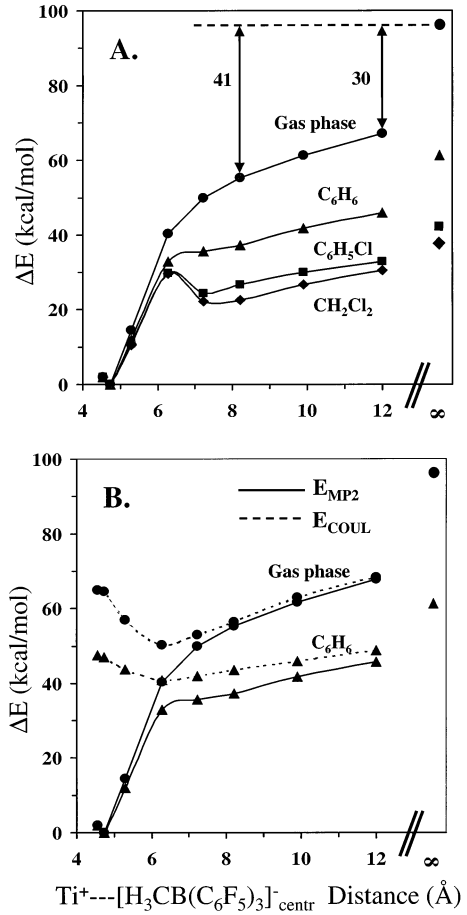

Figure 1. Energetic profile for heterolytic $[H_2Si(C_5H_4)(^tBuN)]TiCH_3^+\cdots H_3CB(C_6F_5)_3^-$ cleavage calculated in the gas phase (MP2) and in benzene, chlorobenzene, and dichloromethane solutions (A). Comparison of gas phase and benzene solution cleavage energetics computed using MP2 quantum chemical methodology and the simple electrostatic interaction of elementary charged particles (B).

located approximately on Ti and the $H_3CB(C_6F_5)_3^-$ centroid. This, in turn, means that the $[H_2Si(C_5H_4)(^tBuN)]TiCH_3^+\cdots H_3CB(C_6F_5)_3^-$ Coulombic interaction along the reaction coordinate during ethylene insertion into the Ti−methyl bond can be straightforwardly estimated and should remain almost inversely proportional to the $Ti^+\cdots[H_3CB(C_6F_5)_3]^-_{centr}$ distance.

The ethylene activation/insertion process at $[H_2Si(C_5H_4)(^tBuN)]TiCH_3^+H_3CB(C_6F_5)_3^-$ involves the μ-CH_3 bonded ion pair ground state structure and, in principle, can proceed via either of three reaction coordinates (Figure 2). Energetic variations and structural modifications along these channels will be analyzed in the following sections.

Energetic and Structure Evolution along Reaction Pathway A. Pathway A involves olefin activation/insertion distal to the $H_3CB(C_6F_5)_3^-$ group. Potential energy profiles as a function of the C(1)−C(13) reaction coordinate are shown in Figure 3, while optimized structures for selected C(1)−C(13) distances are reported in Figure 4. The potential energy surfaces are generally rather flat in the early stages of the reaction (C(1)−C(13) > 3 Å) with the shallow minimum at ~3.20 Å due to van der Waals and dipolar interactions. There is no evidence for formation of a stable π-olefin complex

(30) (a) Rablen, P. R.; Pearlman, S. A.; Miller, D. A. *J. Am. Chem. Soc.* **1999**, *121*, 227. (b) Foresman, J. B.; Keith, T. A.; Wiberg, K. B.; Snoonian, J.; Frisch, M. J. *J. Phys. Chem.* **1996**, *100*, 16098. (c) Foresman, J. B.; Frisch, E. *Exploring Chemistry with Electronic Structure Methods*; Gaussian Inc.: Pittsburgh, PA, 1993.

(31) Frisch, M. J.; Trucks, G. W.; Schlegel, H. B.; Gill, P. M. W.; Johnson, B. G.; Robb, M. A.; Cheeseman, J. R.; Keith, T. A.; Petersson, G. A.; Montgomery, J. A.; Raghavachari, K.; Al-Laham, M. A.; Zakrzewski, V. G.; Ortiz, J. V.; Foresman, J. B.; Cioslowski, J.; Stefanov, B. B.; Nanayakkara, A.; Challcombe, M.; Peng, C. J.; Ayala, P. Y.; Chen, W.; Wong, M. W.; Andres, J. L.; Replogle, E. E. S.; Gomperts, R.; Martin, R. L.; Fox, D. J.; Binkley, J. S.; Defrees, D. J.; Baker, J.; Stewart, J. P.; Head-Gordon, M.; Gonzalez, C.; Pople, J. A. *GAUSSIAN-94*, Gaussian Inc.: Pittsburgh, PA, 1995.

(32) Figure 1A is taken from data previously reported in ref 23b. The abscisa scale is the distance between the Ti and the geometrical centroid of the $CH_3B(C_6F_5)_3^-$ group instead of the Ti···C(2) distance, and the energy differences are not corrected for the basis set superposition error.

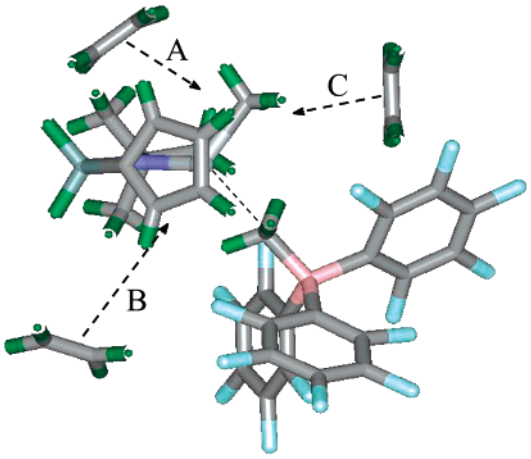

Figure 2. Schematic view of possible pathways for ethylene insertion at the $[H_2Si(C_5H_4)(^tBuN)]TiCH_3^+H_3CB(C_6F_5)_3^-$ contact ion pair.

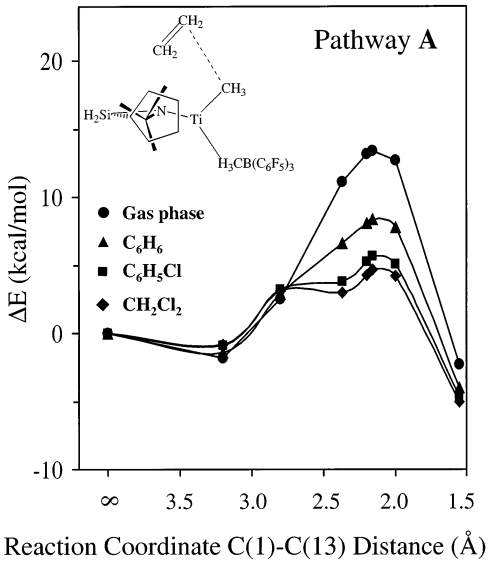

Figure 3. Energetic profile for C_2H_4 activation/insertion at the $[H_2Si(C_5H_4)(^tBuN)]TiCH_3^+H_3CB(C_6F_5)_3^-$ ion pair along pathway A calculated in the gas phase (MP2) and in benzene, chlorobenzene, and dichloromethane solutions.

along pathway A, and the insertion occurs in a single concerted process because the required stretching of the strong $Ti^+\cdots H_3CB(C_6F_5)_3^-$ bond (Figure 1) cannot be energetically compensated by the weaker ethylene complexation. The transition state occurs at C(1)−C(13) = 2.16 Å with a barrier of 13 kcal/mol (Table 1). Nonspecific solvation effects reduce the barrier, and in the case of benzene, an 8 kcal/mol barrier is computed (Table 1). Sizable lowering of the energetic barriers is observed upon increasing solvent polarity, with 6 and 5 kcal/mol barriers calculated for pathway A in chlorobenzene and dichloromethane, respectively.

The immediate kinetic insertion product (C(1)−C(13) = 1.55 Å) is slightly more stable than the reactants ($\Delta E \sim -2$ kcal/mol); however, it undergoes rearrangement to more stable (∼ −22 kcal/mol) structures having different *n*-propyl chain conformations (vide infra). The ΔE (−24 kcal/mol) associated with the overall insertion is consistent with the energy released when a C=C π bond is transformed into a C−C σ bond ($\Delta H \approx -20$ kcal/mol). Relative to the related naked cation, the overall insertion process is less exothermic (∼10 kcal/mol) due to the lack of the additional β- or γ-agostic interactions present in the metal-propyl naked cation.[23a]

In the early stages (e.g., C(1)−C(13) = 2.80 Å) of the insertion (Figure 3), the interactions are largely repulsive since the $H_3CB(C_6F_5)_3^-$ group still remains strongly bound to the electrophilic metal center and leaves little room for the approaching ethylene molecule. At this stage (Figure 4), no major structural modifications occur in the contact ion pair, and the $Ti^+-[H_3CB(C_6F_5)_3]^-_{centr}$ distance remains nearly the same as in the reactants (4.72 vs 4.75 Å). As the ethylene approaches the metal center, the Ti−C(1)H_3 vector bends toward the Ti−N−Si plane and, simultaneously, the $Ti\cdots H_3CB(C_6F_5)_3^-$ contact undergoes major lengthening. This reorganization has the effect of reducing the anion−olefin steric repulsion and increasing both the partial charge separation and the metal electrophilicity, thus "preparing" the Ti atom for the subsequent olefin insertion process.

At the transition state, the $Ti^+\cdots[H_3CB(C_6F_5)_3]^-_{centr}$ distance is 6.62 Å, while the Ti−C(1)H_3 vector is now bent 33° out of the Ti−N−Si plane and on the opposite side of the plane relative to the initial position. The four-membered Ti−C(1)−C(13)−C(12) metallacycle structure is found in the related naked cation calculations[23a] and exhibits a highly distorted (relative to C_{3v}) conformation of the Ti−C(1)H_3 hydrogen atoms. Two C−H bonds are pseudo-eclipsed with respect to the ethylene fragment, while the third engages in some degree of α-agostic interaction with the Ti^+center (Ti··· H = 2.11 Å). Some puckering of the four-membered ring (11°) is also evident. Similar to the results for the naked cation reaction pathways,[23a] the transition state involves formation of a new metal−ethylene σ bond (Ti−C(12) = 2.18 Å) and partial breaking of both ethylene−π ($\Delta C(12)-C(13) = +0.09$ Å) and Ti−methyl (ΔTi−C(1) = +0.09 Å) bonds, asynchronously with the alkyl chain lengthening, since the long C(1)−C(13) distance (2.16 Å) is still indicative of a very weak interaction at this point.

Interesting structural changes are also observed in the $H_3CB(C_6F_5)_3^-$ fragment at the pathway A transition state. The $H_3C-B(C_6F_5)_3^-$ bond distance is shorter than the initial value (1.64 vs 1.71 Å), and the average ∠H−C(2)−B lies close to tetrahedral (111.3° average). Both parameters are similar to those in the free $H_3CB(C_6F_5)_3^-$ anion ($H_3C-B(C_6F_5)_3^-$ = 1.65 Å and ∠H−C(2)−B = 111.6°).[13b] Analogously, the computed B−C(C_6F_5) bond distances (1.68 Å average) and the C(2)−B−C(C_6F_5) bond angles (109.5° average) resemble those found in the free $H_3CB(C_6F_5)_3^-$ anion (1.68 Å and 108.3°, respectively). These geometrical features and the computed charge on the $H_3CB(C_6F_5)_3^-$ group (−0.93 eu) indicate a largely dissociated ion pair. The insertion reaction proceeds along pathway A with the formation of new C(1)−C(13) and Ti−C(12) bonds and complete scission of the Ti−C(1) bond. After insertion is complete, the $H_3CB(C_6F_5)_3^-$ anion translates back toward the Ti center, although the $Ti^+\cdots[H_3CB(C_6F_5)_3]^-_{centr}$ distance (5.48 Å) in the kinetic insertion product is somewhat longer than in the reactants (4.75 Å; Figure 4). The conformation of the *n*-propyl chain indicates γ-agostic interactions similar to those in the naked $[H_2Si(C_5H_4)(^tBuN)]Ti(n\text{-propyl})$ cation.[23] These interactions, however, are much weaker (longer Ti···C(1)H_3 contact, =

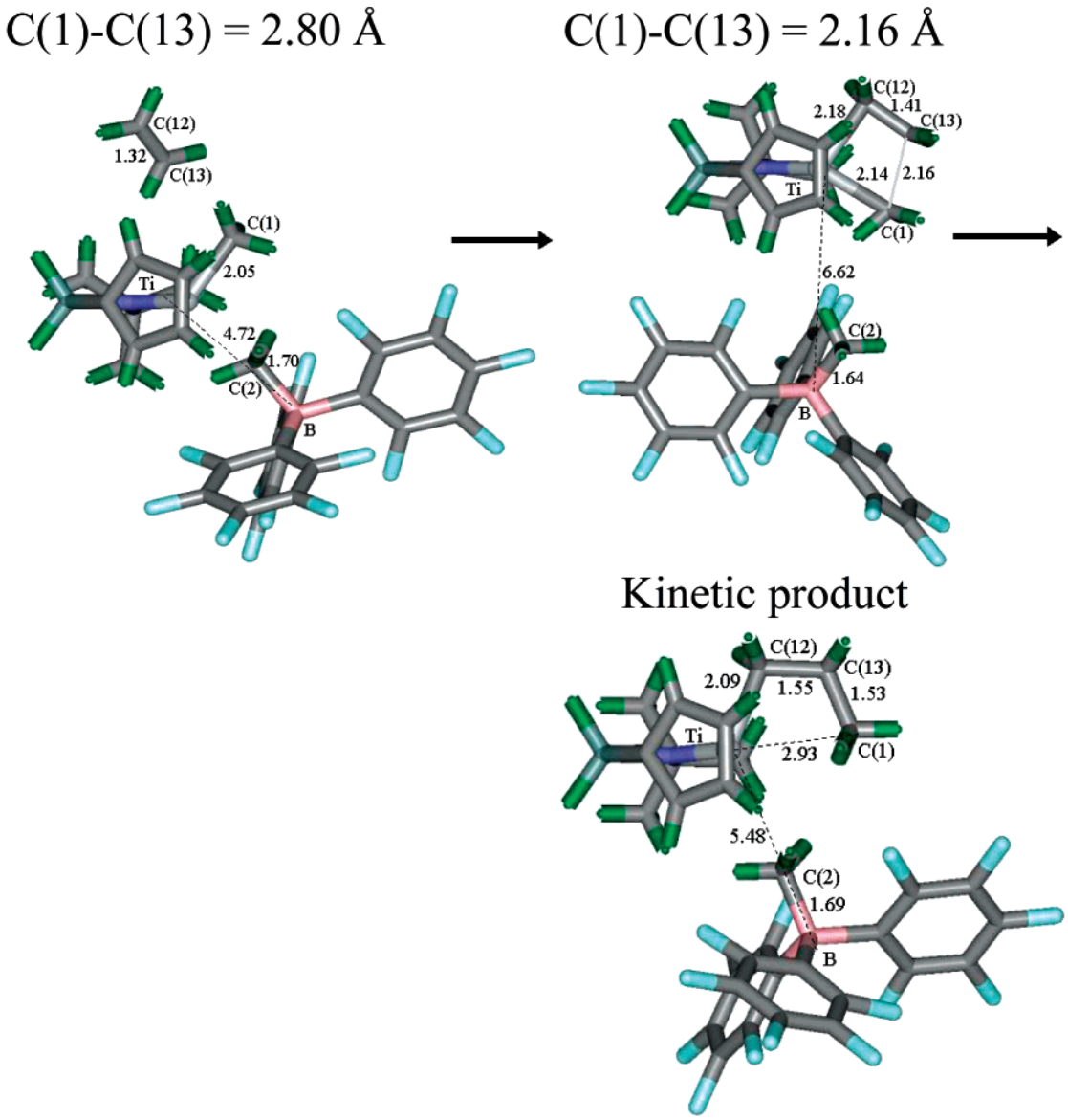

Figure 4. Selected optimized molecular structures along insertion reaction pathway A.

Table 1. Relative Energies (kcal/mol) of Transition States and Intermediates (π-Ethylene Complex) along the Reaction Channels Shown in Figure 2[a]

	pathway A			pathway B				pathway C	
	TS	kinetic product	final product	**TS-I**	π-complex	**TS-II**	kinetic product	**TS-I**	π-complex
gas-phase	13 (14)[b]	−2	−24	12	6 (5)[b]	15 (13)[b]	7	7	5
C_6H_6	8	−4	−24	9	2	10	2	6	2
C_6H_5Cl	6	−5	−24	7	0	8	−1	5	0
CH_2Cl_2	5	−5	−24	6	−1	7	−2	5	−1

[a] The energies of the isolated reagents are always assumed as reference for the energy scale. [b] Values in parentheses refer to B3LYP/B3LYP results.

2.93 Å; larger ∠Ti−C(12)−C(13) = 109.7°, close to the undistorted sp^3 value) due to the reduced electrophilicity of the metal center as a consequence of the closer $H_3CB(C_6F_5)_3^-$ anion approach, which transfers electron density to the $[H_2Si(C_5H_4)(^tBuN)]TiCH_3^+$ cation (+0.81 vs +1.00 eu in the naked cation). This structure readily rearranges to more stable conformations, as will be discussed later.

Energetic and Structure Evolution along Reaction Pathways B and C. In pathway B, the ethylene activation/insertion directly intrudes into the $Ti^+\cdots H_3CB(C_6F_5)_3^-$ framework space volume, engendering greater congestion. The potential surface along the C(1)−C(13) reaction coordinate (Figure 5) exhibits three minima associated with the van der Waals contact species (C(1)−C(13) = 6.00 Å), an intermediate π-ethylene complex (C(1)−C(13) = 3.24 Å), and the kinetic insertion product (C(1)−C(13) = 1.57 Å). Two distinct energetic maxima at ∼4 Å (**TS-I**) and 2.14 Å (**TS-II**) are, in addition, observed. The first transition state represents

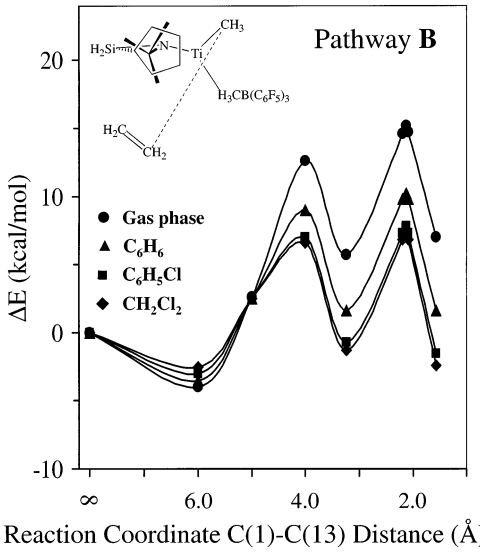

Figure 5. Energetic profile for C_2H_4 activation/insertion at $[H_2Si(C_5H_4)(^tBuN)]TiCH_3^+$ $H_3CB(C_6F_5)_3^-$ along pathway B calculated in the gas phase (MP2) and in benzene, chlorobenzene, and dichloromethane solutions.

Table 2. Bond Lengths (Å) and Bond Angles (deg) of Intermediates and Transition States for Ethylene Insertion into the $[H_2Si(C_5H_4)(^tBuN)]TiCH_3^+H_3CB(C_6F_5)_3^-$ Contact Ion Pair (Pathway B) and the Related Naked Cation

	π-complex		transition state	
	contact ion pair	naked cation[a]	contact ion pair	naked cation[a]
Ti−C(1)	2.04	2.05	2.13	2.16
Ti−C(12)	2.87	2.90	2.14	2.15
Ti−C(13)	2.58	2.64		
C(1)−C(13)	3.24	3.22	2.14	2.13
C(12)−C(13)	1.34	1.34	1.42	1.42
Ti−C(12)−C(13)	63.9	65.2	87.3	87.3
Ti−C(12)−C(13)−C(1)	4.0	4.0	12.1	9.8

[a] Data from ref 23a.

the displacement of the $H_3CB(C_6F_5)_3^-$ counteranion due to the formation of a stable intermediate C_2H_4 π-complex. The second transition state involves the insertion process. Thus, pathway B occurs via a two-step Cossee−Arlman-type process with rate-determining formation of the four-center insertive transition state (**TS-II**). The pathway B potential energy surface is far more sensitive to solvation effects than that of pathway A. The relative energies of both the maxima and minima are sensitive to the solvent dielectric constant because the sizable (even in the early stages) elongation of the $Ti^+\cdots H_3CB(C_6F_5)_3^-$ contact engenders considerable charge separation. Pathway B is not energetically favored with respect to pathway A in the gas phase (**TS-II** $\Delta E = 15$ vs 13 kcal/mol) because of the destabilization arising from the greater cation−anion separation. Nevertheless, the present calculations show that solvents with relatively high dielectric constants stabilize transition states with large charge separations, thereby rendering pathway B competitive with pathway A.

Molecular geometries along pathway B exhibit qualitative similarities to the ethylene insertion reaction coordinate involving the parent $[H_2Si(C_5H_4)(^tBuN)]TiCH_3^+$ naked cation (Table 2),[23a] and therefore, comparison of pertinent energetic data upon moving from the simpler naked cation to the ion pair in the gas phase, and, finally, to the solvated system, allows partitioning of effects due to metal active site versus those due to counteranion and solvent as shown below (Tables 1 and 3 and Scheme 1). Formation of the π-complex is strongly exothermic ($\Delta E_1 \approx -30$ kcal/mol) in the naked cation,[23a] while it is endothermic along pathway B ($\Delta E_1 \approx 6$ kcal/mol), arguing that the energy difference ($\Delta\Delta E_1 \approx 36$ kcal/mol) is primarily associated with the displacement of the $H_3CB(C_6F_5)_3^-$ anion as shown below. Inclusion of solvation slightly decreases the endothermicity because of the additional stabilization of the largely separated $[H_2Si(C_5H_4)(^tBuN)]TiCH_3^+\cdots H_3CB(C_6F_5)_3^-$ ion pair (Table 1). The energy difference between the π-complex and the transition state (ΔE_2) in the naked cation (∼8 kcal/mol) is similar to that found along pathway B (∼9 kcal/mol), indicating that only modest energetic demands (∼1 kcal/mol) arise in displacing the $H_3CB(C_6F_5)_3^-$ anion. The energy change associated with the transition state versus the final kinetic product (ΔE_3) is more exothermic (∼4 kcal/mol) for the naked cation than for pathway B, indicating a smaller ion pair separation in the transition state than in the kinetic product. *This analysis clearly indicates that the principal effect of the counteranion is to shift the reaction coordinate to higher energy, depending on the ion pair strength, while the energy profile associated with the π-complex → transition state → kinetic final product transformation mainly reflects the properties of the catalyst naked cation.*

Scheme 1

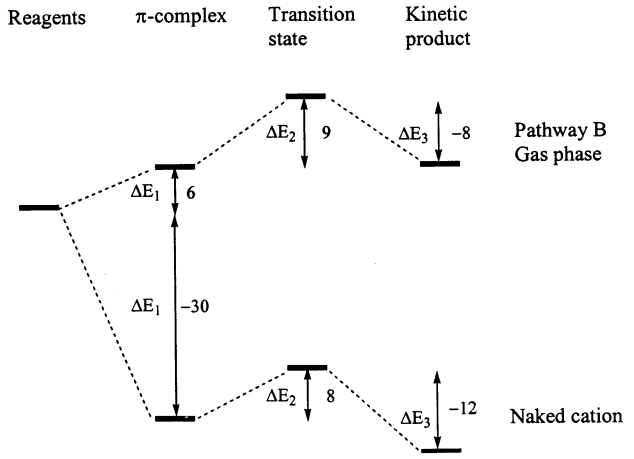

The above trends can be analyzed alternatively using the $Ti^+\cdots[H_3CB(C_6F_5)_3]^-_{centr}$ distance and the coordinates for heterolytic ion pair separation (Figures 1 and 6). The $H_3CB(C_6F_5)_3^-$ group undergoes a major displacement upon C_2H_4 approach and π-complex formation (4.75 vs 6.85 Å). On the basis of the data in Figure 1, $H_3CB(C_6F_5)_3^-$ anion repositioning requires ∼42 kcal/mol, in reasonable agreement with the differing stability (36 kcal/mol) of the π-complex in the naked cation and contact ion pair. Similar $Ti^+\cdots[H_3CB(C_6F_5)_3]^-_{centr}$ separations (6.85 vs 7.08 Å) are observed in the π-complex and transition state. This observation agrees well with the comparable ΔE_2 values computed for both the naked cation and pathway B ($\Delta\Delta E_2 = 1$ kcal/mol). The ΔE_3 energy change ($\Delta\Delta E_3 \approx 4$ kcal/mol) found on passing from the naked cation to the contact ion pair reflects both the energetic demands (1 kcal/mol) of achieving the greater ion pair separation (7.08 vs 7.22 Å) and stronger

Table 3. Potential Energy (ΔE), Standard Enthalpy ($\Delta H°_{298}$), and Free-Energy ($\Delta G°_{298}$) Variations for Ethylene Insertion into the $[H_2Si(C_5H_4)(^tBuN)]TiCH_3^+H_3CB(C_6F_5)_3^-$ Contact Ion Pair (Pathway B) and Related Naked Cation

	π-complex	insertion barrier (π-complex→**TS-II**)	kinetic product
contact ion pair			
ΔE	6	9	7
$\Delta H°_{298}$	7	9	10
$\Delta G°_{298}$	16	12	20
naked cation			
ΔE	−30	8	−34
$\Delta H°_{298}$	−28	8	−30
$\Delta G°_{298}$	−17	11	−18

agostic interactions in the naked cation system. Similar arguments explain the relative stability trends upon moving from the π-complex to transition state and final kinetic product in the gas phase and in benzene solution. In particular, the nearly constant differences (∼5 kcal/mol) parallel similarly constant differences in the computed $Ti^+\cdots[H_3CB(C_6F_5)_3]^-_{centr}$ distances (6.85, 7.08, and 7.22 Å, respectively) which in all cases occupy the flat region of the energy surface describing heterolytic dissociation in benzene (Figure 1). In pathways A and B, the insertion barriers differ (13 vs 15 kcal/mol), in agreement with the greater $Ti^+\cdots[H_3CB(C_6F_5)_3]^-_{centr}$ separation in the two transition states (6.62 vs 7.08 Å). On the basis of Figure 1, this implies an energy difference of ∼3 kcal/mol.

The potential energy variation (ΔE) at key points along the reaction coordinate for ethylene insertion into the contact ion pair (pathway B) and naked cation has also been corrected for zero-point vibrational and thermal energies ($\Delta H°_{298}$) and for entropic ($-T\Delta S$) contributions ($\Delta G°_{298}$, Table 3). Note that ΔE and $\Delta H°_{298}$ are comparable, and only a modest variation is observed for the kinetic product stability in both naked cation and contact ion pair systems. In contrast, the $-T\Delta S$ term significantly affects reaction profiles at higher energies because of the degrees of freedom lost in the ethylene molecule incorporation. This effect is less marked for insertion processes involving the contact ion pairs because the entropy loss accompanying ethylene coordination is partially offset by the entropy increase at greater cation−anion separation.

Geometries and related metrical data along reaction pathway **B** are shown in Figure 6. Even in the early stages, ethylene approach forces the $H_3CB(C_6F_5)_3^-$ group away, with sizable elongation of the $Ti^+\cdots[H_3CB(C_6F_5)_3]^-_{centr}$ contact and formation of a stable olefin π-complex at C(1)−C(13) = 3.24 Å (essentially an olefin-separated ion pair). The structure of the cationic $[H_2Si(C_5H_4)(^tBuN)]TiCH_3\cdot(C_2H_4)^+$ complex is closely reminiscent of the naked cation π-complex, with comparable metrical parameters (Table 2).[23a] The $H_3CB(C_6F_5)_3^-$ anion is located far from the metal center ($Ti^+\cdots[H_3CB(C_6F_5)_3]_{centr}$ = 6.85 Å), and $H_3CB(C_6F_5)_3^-$ metrical parameters as well as the partial charge (−0.92 eu) indicate significant charge separation involving essentially free ions. The ethylene is "sandwiched" between the $[H_2Si(C_5H_4)(^tBuN)]TiCH_3^+$ and $H_3CB(C_6F_5)_3^-$

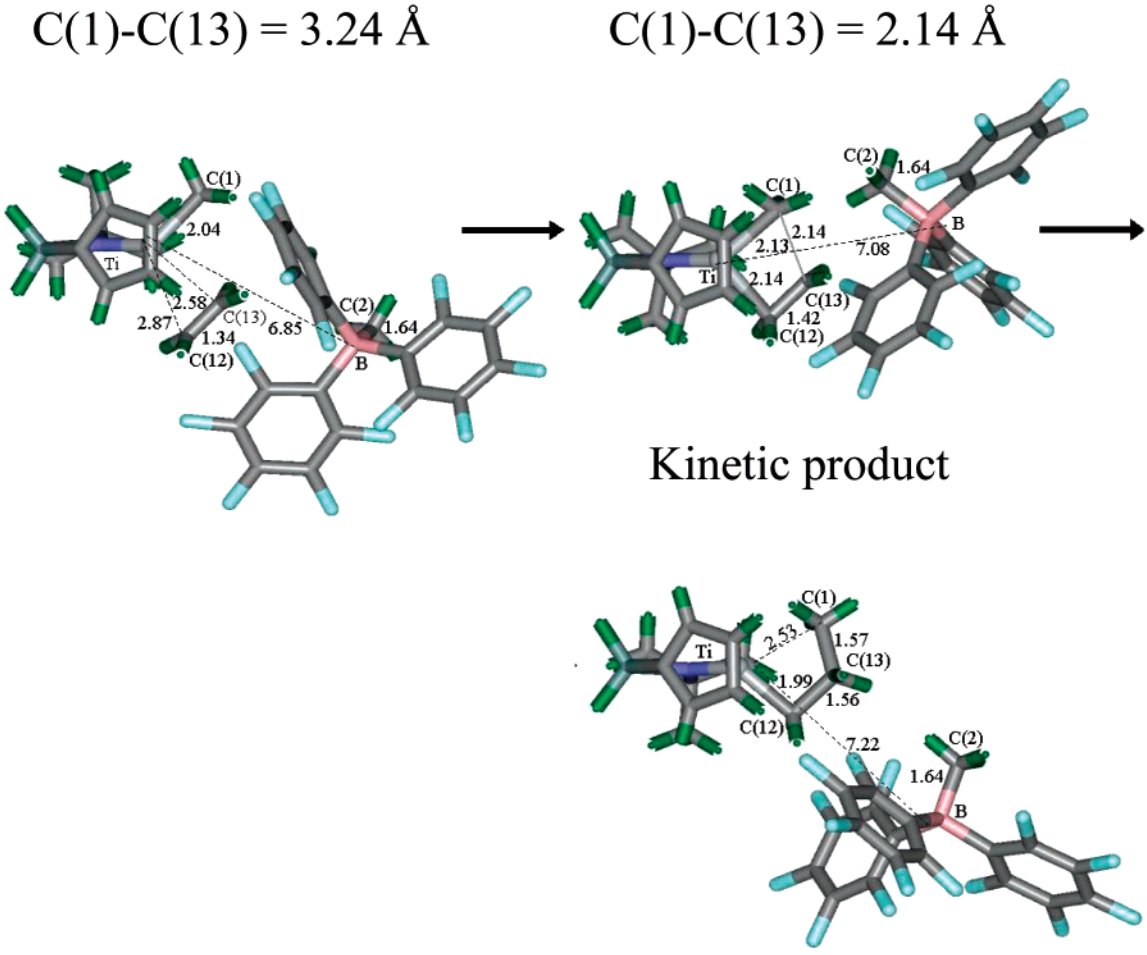

Figure 6. Selected optimized molecular structures along insertion reaction pathway B.

groups, with the consequence that both the Ti−C(12) and Ti−C(13) bond distances are slightly compressed (∼0.04 Å) versus the naked cation due to the "pressure" of the $H_3CB(C_6F_5)_3^-$ counteranion. Similar to the naked cation π-complex, the differing Ti−C(12) and Ti−C(13) Ti-ethylene contacts reflect differing repulsive interactions with either the Cp ring or the ^{t}BuN group, leading to asymmetric bonding.

The pathway B transition state (Figure 5) occurs at C(1)−C(13) = 2.14 Å, and the structure of the metallacycle resembles that found in the naked cation[23a] (Figure 6, Table 2). The Ti−C(12)−C(13)−C(1) ring exhibits a 12.1° folding angle along the C(1)−C(12) internuclear vector and involves a highly distorted $TiC(1)H_3$ conformation compared to that in the π-complex. Two C−H bonds are pseudo-eclipsed with respect to the ethylene fragment, while the third is involved in a strong α-agostic interaction. Note that the latter C(1)−H bond distance is considerably longer (1.11 Å) than the others (1.08 Å), and the related ∠Ti−C(1)−H is markedly contracted (73.5° vs 112.4° and 136.1°). The large $Ti^+\cdots[H_3CB(C_6F_5)_3]^-_{centr}$ contact (7.08 Å), the internal metrical parameters, and the partial computed charge on $H_3CB(C_6F_5)_3^-$ are indicative of essentially complete ion pair dissociation at this point on the reaction coordinate, similar to the structure of the ethylene π-complex. Clearly, substantial repositioning of the $H_3CB(C_6F_5)_3^-$ anion is characteristic of this pathway. In the *n*-propyl kinetic insertion product, the $H_3CB(C_6F_5)_3^-$ anion remains unbound and distant from the metal center. The vacant coordination site is saturated by the *n*-propyl chain, analogously to the situation in pathway A. However, the present structure does not exhibit high stability (Table 1) due to the large $Ti^+\cdots[H_3CB(C_6F_5)_3]^-_{centr}$ separation (7.22 Å). It does, however, feature a sizable γ-agostic interaction between the *n*-propyl alkyl chain and the Ti, similar to that found in the kinetic product of the naked cation. The interplay of energetics and geometrical features will be analyzed in detail in the following section.

Along pathway C, the type of reaction coordinate adopted for pathways A and B is not useful for understanding ethylene coordination since it involves the same space volume as the strongly coordinating $H_3CB(C_6F_5)_3^-$ anion. Thus, the Ti−C(12) distance was adopted to analyze this process (Figure 7). The insertion proceeds to product via an intermediate π-complex and a four-center transition state structure. The energy profile exhibits two maxima and three minima, similar to pathway B. Upon ethylene approach, $H_3CB(C_6F_5)_3^-$ undergoes a sizable displacement concurrent with π-complex formation (Ti−C(12) = 2.92 Å). The ethylene lies between the $[(H_2Si(C_5H_4)(^t\text{BuN})]TiCH_3^+$ cation and the $H_3CB(C_6F_5)_3^-$ counteranion, analogous to pathway B (Figure S1). In this case also, a modest energetic barrier (∼7 kcal/mol at the MP2 level) is found at Ti−C(12) ≈ 3.2 Å, and the relative energy of the π-complex (+5.0 kcal/mol at MP2 level) closely compares to that found for pathway B (+5.8 kcal/mol). The reduced energy barrier for counteranion displacement/ethylene coordination (**TS-I**) along pathway C versus pathway B (7 vs 12 kcal/mol in gas phase) renders the former channel more favorable for the formation of the cation−ethylene−anion sandwich system. The $[H_2Si(C_5H_4)(^t\text{BuN})]$-

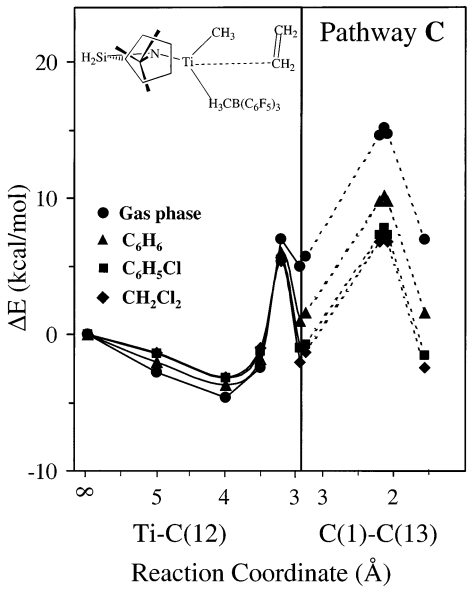

Figure 7. Energetic profile for C_2H_4 activation/insertion at $[H_2Si(C_5H_4)(^t\text{BuN})]TiCH_3^+H_3CB(C_6F_5)_3^-$ along pathway C calculated in the gas phase (MP2) and in benzene, chlorobenzene, and dichloromethane solutions. The initial stage of the reaction profile (reagents→ transition state I → π-complex) was computed using the internuclear vector along the evolving Ti−C σ bond ($CH_3Ti\cdots CH_2{=}CH_2$) as the reaction coordinate (solid lines). The remaining energy profile curves (π-complex → transition state II → kinetic product) were assumed to be the same as in pathway B (dashed lines).

$TiCH_3{\cdot}C_2H_4^+$ cation geometry is similar to the π-complex along pathway B even though positioning of the $H_3CB(C_6F_5)_3^-$ anion is different. Note, however, that anion repositioning does not involve drastic total energetic changes since all ion pair structures with different, distant $H_3CB(C_6F_5)_3^-$ positionings lie close in energy. This observation agrees with both the large flexibility and isotropic character of the $Ti^+\cdots H_3CB(C_6F_5)_3^-$ interaction ubiquitous in experimental data on metallocene ion pairs.[7,8,13] *These results indicate that the pathway C insertion coordinate, from π-complex to final kinetic n-propyl product, evolves similarly to pathway B and with a comparable overall barrier (∼15 kcal/mol) at the MP2 level.*

Comparative Structural and Energetic Analysis of Reaction Pathways Using DFT-B3LYP. Starting from the HF optimized structures, the geometries of significant points along the ethylene insertion reaction channels (pathways A and B) were also computed at the DFT-B3LYP level to assess the role of electron correlation. The resulting structures are very similar to those obtained at the HF level (Figures 4 and 6), and relevant metrical parameters for reactants, intermediate π-complexes (pathway B), and transition states (pathways A and B) are compared in Table 4. For all B3LYP optimized structures, the only significant metrical difference is modest Ti−$[H_3CB(C_6F_5)_3]_{centr}$ contact shortening, the magnitude of which depends on the structure and ranges from 0.03 to 0.28 Å. Thus, inclusion of electron correlation results in a slight contraction of the interionic distance. Upon proceeding to the B3LYP optimized geometry, the Ti−C_2H_4 distances for the intermediate π-complex (pathway B) also shorten slightly with a ∼0.08 Å contraction in Ti−C(12) and Ti−C(13).

Table 4. Computed RHF vs DFT-B3LYP (in Parentheses) Selected Bond Lengths (Å) and Bond Angles (deg) of $H_2Si(C_5H_4)(^tBuN)TiCH_3^+H_3CB(C_6F_5)_3^-$ and C_2H_4 Reagents, Intermediate (Pathway B), and Transition States (Pathways A and B)[a]

	reagents	transition state pathway A	π-complex pathway B	transition state pathway B
Ti−C(1)	2.05 (2.07)	2.14 (2.11)	2.04 (2.05)	2.13 (2.09)
Ti−C(12)		2.18 (2.24)	2.87 (2.81)	2.14 (2.22)
Ti−C(13)			2.58 (2.46)	
C(1)−C(13)		2.16 (2.20)	3.24 (3.36)	2.14 (2.20))
C(12)−C(13)	1.32 (1.34)	1.41 (1.41)	1.34 (1.35)	1.42 (1.41)
$Ti-[H_3CB(C_6F_5)_3]^-_{centr}$	4.75 (4.66)	6.62 (6.41)	6.85 (6.57)	7.08 (7.05)
C(2)−B	1.70 (1.70)	1.64 (1.65)	1.64 (1.65)	1.64 (1.64)
θ[b]	53.2 (56.4)	32.7 (31.3)	44.2 (52.9)	39.1 (33.4)
Ti−C(12)−C(13)		86.5 (83.5)	63.9 (61.2)	87.3 (83.8)
Φ[c]		7.8 (9.9)	4.0 (5.3)	12.1 (9.5)

[a] Atom labeling defined in Figures 4 and 6. [b] θ defines the angle between the plane Cp_{centr}−Ti−N and the Ti−C(1) vector. [c] Φ indicates the Ti−C(12)−C(13)−C(1) torsional angle.

These small geometrical changes presumably reflect slightly enhanced C_2H_4 dative interactions upon introducing electron correlation. For both A and B, the insertive transition state occurs slightly earlier (Δ(C(1)−C(13)) ≈ 0.05 Å) at the B3LYP level. All of these small structural modifications are reminiscent of those on passing from HF to MP2 for the $[H_2Si(C_5H_4)(CH_3N)]$-$Ti(CH_3)^+H_3CBF_3^-$ model (Ti−H_3CBF_3 contracts 0.07 Å),[23c] for the intermediate π-complex (Ti−C_2H_4 contacts shorten by 0.2 Å), and for the transition state (earlier transition state with Δ(C(1)−C(13)) ≈ 0.03 Å) found for ethylene insertion at the $[H_2Si(C_5H_4)(^tBuN)]TiCH_3^+$ naked cation.[23a]

In regard to energetics for ethylene insertion, there is great similarity between the stability of the intermediate π-complex (6 vs 5 kcal/mol), the transition state for pathway B (15 vs 13 kcal/mol), and the transition state for pathway A (13 vs 14 kcal/mol) on passing from MP2/HF to B3LYP/B3LYP. The only noticeable energetic discrepancy is that pathway B, which was disfavored by 2 kcal/mol in MP2/HF, is now preferred by 1 kcal/mol (Table 1). Two factors can explain this minor stability inversion on passing from MP2/HF to B3LYP/B3LYP: (i) structural differences in optimized geometries (HF vs B3LYP), (ii) methodologies in computing total energy (MP2 vs B3LYP). To address this, B3LYP single-point energy calculations were also carried out using HF optimized geometries. In agreement with the B3LYP/B3LYP results, pathway B is found to be energetically preferred over pathway A (∼1 kcal/mol). Therefore, the observed energetic MP2/HF to B3LYP/B3LYP inversion is ascribed to the different methodologies in computing total energies rather than to differences in optimized structures.

Energetics and Structure Analysis of the $[H_2Si(C_5H_4)(^tBuN)]Ti(n\text{-}C_3H_7)^+H_3CB(C_6F_5)_3^-$ Final Insertion Product. Pathway A affords the kinetic insertion product **1** (Figures 4 and 8), which is slightly more stable than the reactants (ΔE = −2 kcal/mol at MP2 level) because the alkyl chain conformation precludes close $H_3CB(C_6F_5)_3^-$ approach to the cationic Ti center. Rearrangements of the *n*-propyl chain by rotation about either the Ti−C(12) or C(12)−C(13) bond incur almost negligible barriers and relieve the steric encumbrance at the vacant metal site, thus allowing closer $H_3CB(C_6F_5)_3^-$ approach. The resulting conformers all lie close in energy, with the $Ti^+\cdots[H_3CB(C_6F_5)_3]^-_{centr}$ contact ∼4.8 Å. In these conformers, the Ti-propyl chain (Ti−C(12)−C(13)−C(1) linkage) twists to an approximately staggered conformation, thus relaxing steric repulsions among CH_2/CH_3 groups. The four conformers obtained related by rotations about the Ti−C(12) and C(1)−C(13) bonds (**2**−**5**; Figure 8) are considerably more stable than insertion product **1** (∼−20 kcal/mol), with relative stabilities reflecting various interligand repulsive interactions (Figure 8, Table 5). Thus, rotations about the C(12)−C(13) vector that move the $C(1)H_3$ group closer to the cyclopentadienyl ring result in structure **2**, while closer approach of the $C(1)H_3$ group to the ^{t}Bu group affords final ground state structure **3**, considerably different in geometry than **1** (Figure 9). Rotations about the Ti−C(12) vector induce a closer approach of the *n*-propyl $C(13)H_2C(1)H_3$ terminus either to the Cp ring (structure **4**) or to the ^{t}BuN group, leading to **5**. Finally, stable structure **6** has the $C(13)H_2C(1)H_3$ group lying near the C(2)−Ti−C(12) plane, minimizing propyl steric repulsions with both Cp and amido ligands.

Possible interactions involving metallocenium- -perfluorarylborate coordination via metal···fluorine(aryl) contacts[7d,8c,h,10a] were also analyzed. Similar to the $[H_2Si(C_5H_4)(^tBuN)]TiCH_3^+H_3CB(C_6F_5)_3^-$ ion pair discussed above, several energetically accessible structures were located for $[H_2Si(C_5H_4)(^tBuN)]TiC_3H_7^+H_3CB(C_6F_5)_3^-$. However, all lie somewhat higher in energy than μ-CH_3 coordination. For example, structure **7** (Figure 9) is ∼3 kcal/mol less stable than **6** at the MP2 level. Comparison of the relative stabilities of ground state conformations of the methyl and *n*-propyl derivatives reveals that, upon alkyl chain homologation, there is a *greater tendency* for Ti···F coordination. This is supported both by the shorter computed Ti···F bond distance in the *n*-propyl species versus that in the methyl analogue (2.07 vs 2.08 Å) and by the greater C−F elongation (C−F = 1.44 vs 1.42 Å, respectively).

Along pathway B, final insertion product **8** (Figure 6) has a considerably longer $[H_2Si(C_5H_4)(^tBuN)]$-$TiC_3H_7^+\cdots H_3CB(C_6F_5)_3^-$ contact ($Ti^+\cdots[H_3CB(C_6F_5)_3]_{centr}$ = 7.22 Å) than most of the final ion pair structures discussed above, and the *n*-propyl chain interacts in a γ-agostic fashion with the metal center (Ti···C(1) = 2.53 Å; C(1)−C(13) = 1.57 Å), similar to the kinetic product in the parent naked cation (Ti···C(1) = 2.65 Å; C(1)−C(13) = 1.55 Å).[23a] Conformer **8** can undergo rearrangement upon rotation (∼120°) about the C(12)−C(13) bond, and two different optimized structures are obtained (**9**, **10**; Figure S2). Both exhibit significant agostic interactions involving the C(13)−H bond (Ti···HC(13) ≈ 2.10 Å; H−C(13) = 1.14 Å), similar to β-agostic

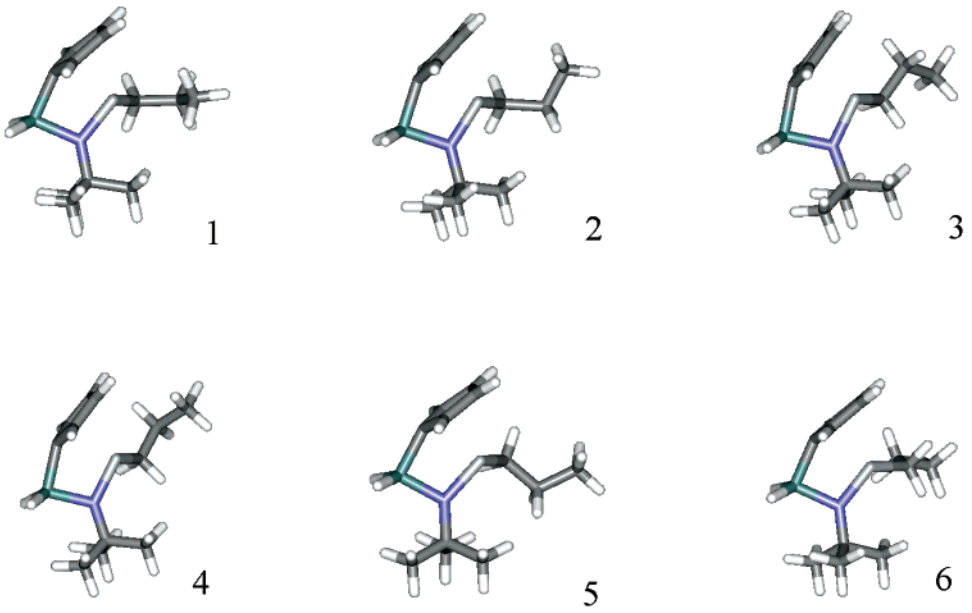

Figure 8. Optimized structures of the $[H_2Si(C_5H_4)(^tBuN)]Ti(n\text{-}C_3H_7)^+$ $H_3CB(C_6F_5)_3^-$ contact ion pair. The $CH_3B(C_6F_5)_3^-$ counteranion is omitted for ease of viewing.

structures found in the related naked cation (Ti···HC(13) = 2.11 Å; H−C(13) = 1.14 Å). Structures **8**, **9**, and **10** have comparable energetic stabilities, even though the $H_3CB(C_6F_5)_3^-$ anion is positioned differently, in all cases distal to the *n*-propyl chain. Furthermore, structures **8**, **9**, and **10** have lower stabilities than **2**−**6** in pathway A and do not evolve spontaneously to more stable geometries (no imaginary frequency in vibrational analysis). This is clearly indicative of substantial counteranion mobility and of the very flat structural potential energy surface arising from the large residual Coulombic interactions still operative over large ion pair separations. Because of the importance of these two kinds of structures (**2**−**6** and **8**−**10**) in the catalytic polymerization processes (vide infra), relative stabilities were investigated in greater detail for two representative cases (**3** and **8**), including both solvent and free energy effects (Table 6). It is evident that solvation has dramatic effects on the energetics because it preferentially stabilizes structures having large cation−anion separations. Similarly, structures with extended $H_2Si(C_5H_4)(^tBuN)TiC_3H_7^+\cdots H_3CB(C_6F_5)_3^-$ contacts are entropically favored because of the greater degrees of freedom. Table 6 summarizes the energies required for total ion pair separation as a function of solvent polarity, including entropic effects. Note that if C_6H_5Cl and CH_2Cl_2 are used as solvents, almost complete ion pair separation is achieved ($\Delta G°_{298}$ = 7 and 4 kcal/mol, respectively). Structures having agostic interactions have been postulated as key intermediates in metallocene-based Ziegler−Natta catalysis;[1] however up to now the evidence has largely been based on experimental kinetic isotope effect data.[33] The present results

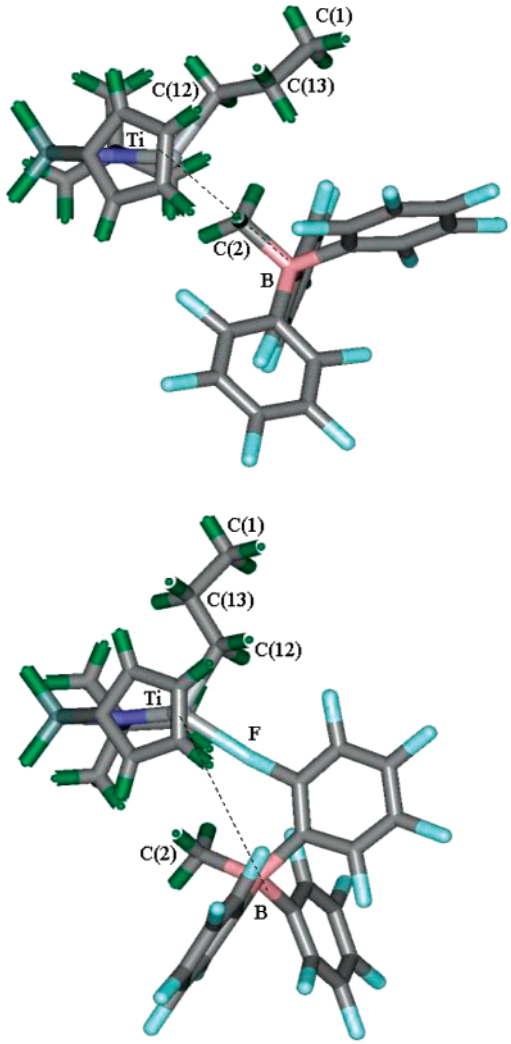

Figure 9. Molecular structures of the $[H_2Si(C_5H_4)(^tBuN)]Ti(n\text{-}C_3H_7)^+H_3CB(C_6F_5)_3^-$ contact ion pair in the ground state conformation **3** (top) and in which an aryl fluorine atom coordinates to metal center **7** (bottom).

(33) (a) Prosenc, M. H.; Brintzinger, H. H. *Organometallics* **1997**, *16*, 3889−3894. (b) Grubbs, R. H.; Coates, G. W. *Acc. Chem. Res.* **1996**, *29*, 85−93. (c) Prosenc, M. H.; Janiak, C.; Brintzinger, H. H. *Organometallics* **1992**, *11*, 4036−4041. (d) Cotter, W. D.; Bercaw, J. E. *J. Organomet. Chem.* **1991**, *417*, C1−C6. (e) Krauledat, H.; Brintzinger, H. H. *Angew. Chem., Int. Ed. Engl.* **1990**, *29*, 1412−1413. (f) Piers, W. E.; Bercaw, J. E. *J. Am. Chem. Soc.* **1990**, *112*, 9406−9407. (g) Jordan, R. F.; Bradley, P. K.; Baenziger, N. C.; LaPointe, R. E. *J. Am. Chem. Soc.* **1990**, *12*, 1289.

Table 5. Energies (kcal/mol) and Selected Bond Lengths (Å) and Bond Angles (deg) of Various Conformations of the $[H_2Si(C_5H_4)(^tBuN)]Ti(n\text{-}C_3H_7)^+H_3CB(C_6F_5)_3^-$ Final Product[a]

	ΔE	Ti−Cp_{centr}	Ti−N	Ti−C(12)	Ti−$[H_3CB(C_6F_5)_3]_{centr}$	Cp_{centr}−Ti−N	Ti−C(12)−C(13)	Ti−C(12)−C(13)−C(1)	N−Ti−C(12)−C(13)	θ^b
1	22.2	2.12	1.86	2.09	5.48	108.8	109.7	1.6	128.8	60.9
2	4.0	2.13	1.88	2.09	4.85	108.9	117.3	76.9	115.1	57.4
3	0.0	2.13	1.88	2.06	4.80	109.6	118.6	160.7	176.3	56.0
4	0.2	2.13	1.88	2.07	4.81	109.4	124.6	56.2	168.9	56.9
5	4.2	2.13	1.88	2.08	4.82	109.4	118.7	99.7	83.2	59.0
6	0.6	2.11	1.88	2.06	4.79	109.6	123.0	171.4	63.7	50.8
7	3.7	2.13	1.87	2.05	5.24	109.7	123.7	169.7	44.9	54.6
8	31.4	2.10	1.87	1.99	7.22	111.0	91.0	32.1	131.9	43.3
		(2.10)[c]	(1.85)	(2.02)		(110.9)	(96.4)	(31.7)	(128.9)	(36.1)
9	33.4	2.08	1.87	2.00	7.07	111.7	87.9	133.1	103.9	17.7
		(2.08)	(1.85)	(2.02)		(111.3)	(88.4)	(139.8)	(106.2)	(19.2)
10	34.4	2.09	1.86	2.01	7.71	111.6	87.8	118.4	94.6	16.2
		(2.08)	(1.85)	(2.02)		(111.7)	(88.1)	(121.4)	(97.6)	(16.8)

[a] Atom labeling defined in Figures 4, 6, 9, and S2. [b] θ defines the angle between the plane Cp_{centr}−Ti−N and the Ti−C(12) vector. [c] Values in parentheses refer to homologues structures of the $H_2Si(C_5H_4)(^tBuN)TiC_3H_7^+$ naked cation system.

Table 6. Relative Stability of the $H_2Si(C_5H_4)(^tBuN)Ti(n\text{-}C_3H_7)^+CH_3B(C_6F_5)_3^-$ Contact Ion Pair in Conformation 3 (Ground State), 8, and Isolated Cation and Anion Including Solvent Effects and Thermal and Entopic Terms

	gas phase		C_6H_6		C_6H_5Cl		CH_2Cl_2	
structure	ΔE	$\Delta G°_{298}$	ΔE	$\Delta G°_{298}$	ΔE	$\Delta G°_{298}$	ΔE	$\Delta G°_{298}$
3	0	0	0	0	0	0	0	0
8	31	29	25	23	22	20	21	19
isolated ions[a]	74	58	40	24	23	7	20	4

[a] Data from ref 23b.

strongly support the existence of stable structures having strong agostic interactions with the counteranion remote to the metal coordination sphere and therefore represent possible resting states for subsequent olefin insertion.

Energetic and Structure Evolution for Ethylene Insertion at the $H_2Si(C_5H_4)(^tBuN)Ti(n\text{-}C_3H_7)^+H_3CB(C_6F_5)_3^-$ Contact Ion Pair. A full analysis of ethylene insertion in contact ion pairs having longer alkyl chains is not a simple task because insertion can occur along several pathways depending on (i) the $H_3CB(C_6F_5)_3^-$ counteranion position (short or long Ti- -$[H_3CB(C_6F_5)_3]_{centr}$ contacts) in the ion pair resting state; (ii) the polymer chain conformation in the ion pair resting state and during insertion; and (iii) the position of ethylene with respect to both chain and counteranion. Even though it is presently impracticable to carry out a full analysis of all possible reaction channels, important insights into how steric and electronic effects associated with a larger alkyl group and, by inference, polymer chain affect ion pairing and the insertive transition state can be obtained by computing the geometries and stabilities of kinetically significant points on a representative reaction coordinate. We chose to study the energetic profile for ethylene insertion at the $H_2Si(C_5H_4)(^tBuN)$-$TiC_3H_7^+H_3CB(C_6F_5)_3^-$ contact ion pair assuming olefin attack on the same side as the cocatalyst (similar to pathways B and C), while the starting polymer chain conformation is chosen as that found to be most stable for the $H_2Si(C_5H_4)(^tBuN)TiC_3H_7^+H_3CB(C_6F_5)_3^-$ contact ion pair ground state (Table 5). In addition, useful information concerning counteranion-associated electronic and steric effects on ethylene insertion into the Ti−C_3H_7 bond can be obtained by comparing energetic profiles for both the naked cation and contact ion pairs. Therefore, ethylene insertion into the $H_2Si(C_5H_4)(^tBuN)$-

Scheme 2

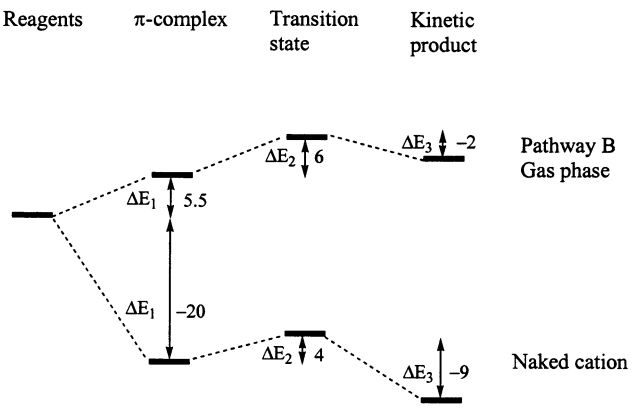

$TiC_3H_7^+$ naked cation was also investigated (Scheme 2, Figure 10, Table 7). In both cases, ethylene insertion is found to proceed through classical ethylene π-complexation, followed by a four-center insertive transition state, and then by formation of an *n*-pentyl γ-agostic kinetic product. However, there are substantial differences between these two energetic profiles. In fact, the π-complex, transition state, and kinetic product for ethylene insertion at the $H_2Si(C_5H_4)(^tBuN)TiC_3H_7^+$ naked cation are located lower in energy than reactants, while these stationary points lie at higher energies for insertion at the contact ion pair because of the energy required for counteranion displacement. A similar situation is observed for the energetic profiles for ethylene insertion into the related Ti−CH_3 bond (vide supra), and thus a comparison will allow separation of long alkyl chain effects on the catalytic active site and on the ion pairing strength.

It is convenient to begin by comparing the energetic profile for ethylene insertion into Ti−CH_3 and Ti−C_3H_7 bonds at both naked cations (Schemes 1 and 2). The stabilization energies for π-complex formation and the γ-agostic Ti-$C_3H_7^+$ kinetic product are ~10 kcal/mol lower (less exothermic) than that obtained for the corresponding Ti-CH_3 cation. This is mainly due to endothermic disruption of the strong γ-agostic interaction in $H_2Si(C_5H_4)(^tBuN)TiC_3H_7^+$. In fact, the Ti-$CH_3$ naked cation has a free metal coordination site that can be readily occupied by ethylene, while in contrast, the vacant metal coordination site in the Ti−$C_3H_7^+$ naked cation is engaged by the terminal CH_3 group in a strong γ-agostic interaction that must be dissociated during

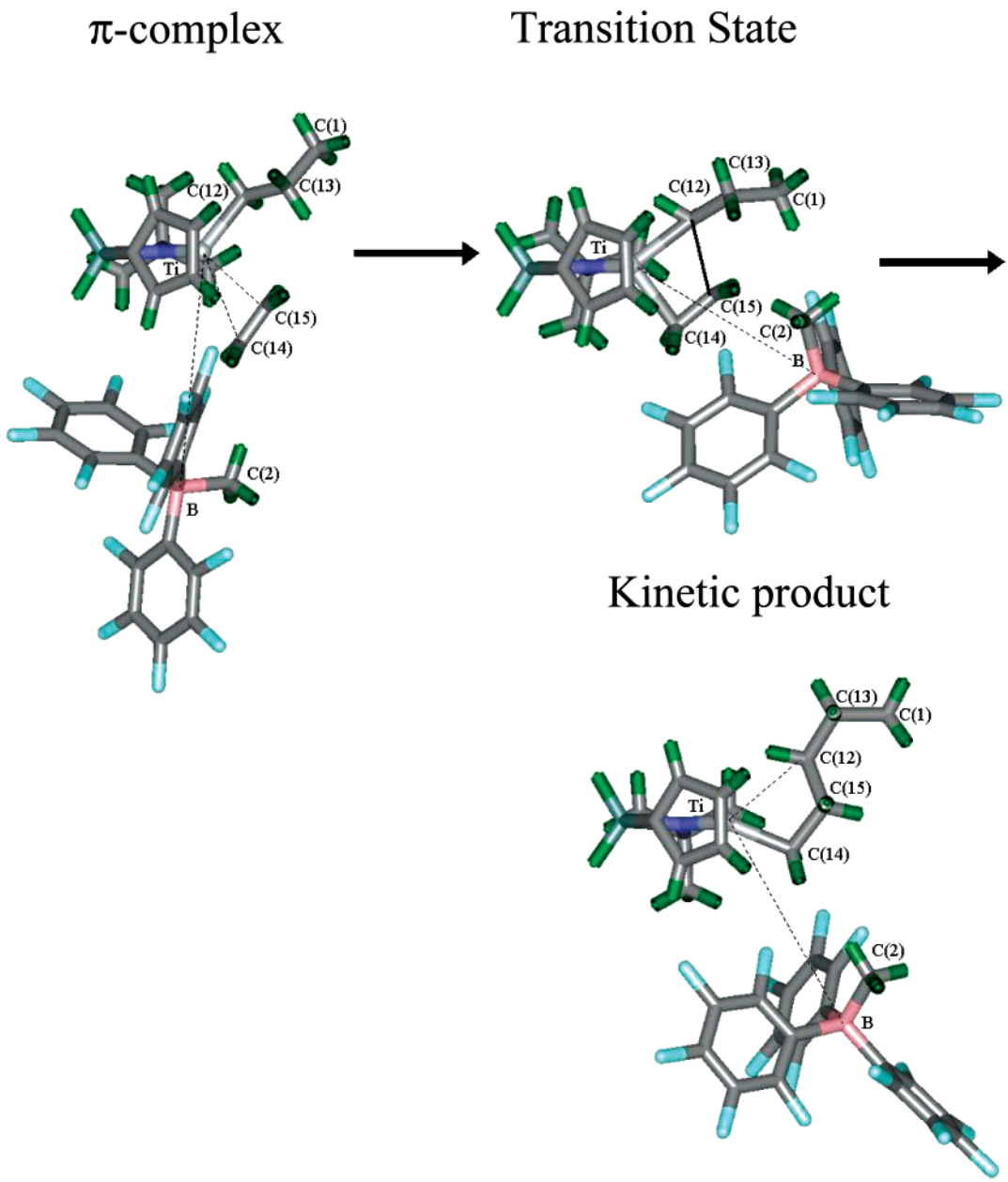

Figure 10. Selected optimized molecular structures for ethylene insertion at the $[H_2Si(C_5H_4)(^tBuN)]Ti(n\text{-}C_3H_7)^+H_3CB(C_6F_5)_3^-$ ion pair.

Table 7. Bond Lengths (Å) and Bond Angles (deg) of Intermediates, Transition States, and Kinetic Products for Ethylene Insertion into the $H_2Si(C_5H_4)(^tBuN)Ti(n\text{-}C_3H_7)^+H_3CB(C_6F_5)_3^-$ Contact Ion Pair and Related $H_2Si(C_5H_4)(^tBuN)Ti(n\text{-}C_3H_7)^+$ Naked Cation[a]

	π-complex		transition state		γ-agostic	
	contact ion pair	naked cation	contact ion pair	naked cation	contact ion pair	naked cation
Ti−C(12)	2.06	2.05	2.14	2.15	2.90	2.77
Ti−C(14)	2.94	2.93	2.15	2.18	2.01	2.03
Ti−C(15)	2.50	2.61				
C(12)−C(15)	3.26	3.31	2.19	2.21	1.54	1.55
C(14)−C(15)	1.34	1.34	1.41	1.41	1.55	1.55
$Ti-[H_3CB(C_6F_5)_3]^-_{centr}$	7.36		7.37		6.85	
C(2)−B	1.64		1.64		1.64	
θ^b	48.9	46.0	34.9	35.5	23.8	33.3
Ti−C(14)−C(15)	58.2	62.9	86.4	85.8	103.5	98.6
Φ^c	8.3	8.8	10.0	8.3	42.0	38.5

[a] Atom labeling defined in Figure 10. [b] θ defines the angle between the plane Cp_{centr}−Ti−N and the Ti−C(12) vector (for π-complex and transition state) or the Ti−C(14) (for kinetic product). [c] Φ indicates the Ti−C(14)−C(15)−C(12) torsional angle.

ethylene complexation. Another factor that reduces the exothermicity of the reaction profile for the $Ti-C_3H_7^+$ cation is the lower Lewis acidity of the metal center due to the presence of a more efficient electron-releasing group, which slightly reduces $Ti\cdots C_2H_4$ and $Ti\cdots C_\gamma$ dative interactions in the $H_2Si(C_5H_4)(^tBuN)TiC_3H_7$·

$(C_2H_4)^+$ π-complex and in the $H_2Si(C_5H_4)(^tBuN)TiC_5H_{11}^+$ γ-agostic kinetic product (the $Ti\cdots C_\gamma$ contact and $\angle Ti-C_\alpha-C_\beta$ increase by 0.12 Å and 2.2°, respectively).

The most interesting aspect of the comparative energetic profiles for the first and second ethylene insertion is clearly the reduction of the insertion energy barrier (the required π-complex → transition state energy decreases from 8 to 4 kcal/mol), indicating that propagation is faster than the initiation step at $Ti-CH_3^+$. Consistent with the lower energy barrier, the computed geometrical parameters for the four-membered $\overline{Ti-CH_2-CH_2-C_3H_7}$ metallacyclic structure indicate an earlier transition state than in the $\overline{Ti-CH_2-CH_2-CH_3}$ structure. In fact, the $H_2Si(C_5H_4)(^tBuN)Ti(C_3H_7)\cdot C_2H_4^+$ transition state occurs at a 0.05 Å longer C−C reaction coordinate, while the olefin C=C bond length is 0.01 Å shorter. The greater electron-releasing and sterically demanding chain produces two important effects in the intermediate π-complex: (i) ethylene coordination is weaker, thus rendering the olefin more available for insertion; (ii) a weak α-agostic interaction ($\angle Ti-C(12)-H = 106°$) induces a $Ti-CH_2$ spatial orientation more suitable for reaching the transition state geometry.

The present results are in general agreement with results reported previously for ethylene insertion at other L_2MR^+ (R = CH_3, C_2H_5, n-C_3H_7, and n-C_5H_{11}) naked cations.[18,19] These studies found shallow energetic minima for π-complex formation and γ-agostic products with a substantial reduction of the insertive energy barriers when the metal-bound alkyl chain becomes longer than CH_3. Thus, Rytter et al.[19b] reported a π-complexation energy and insertion barrier of ∼−15 and ∼6 kcal/mol, respectively, for $(C_5H_5)_2ZrCH_3^+$, while these quantities become ∼−7 and ∼2.5 kcal/mol for $(C_5H_5)_2ZrC_3H_7^+$. Similarly, Zeigler et al.[18g] reported a π-complexation energy and an insertion barrier of −20.8 and 3.8 kcal/mol, respectively, for ethylene insertion at $H_2Si(C_5H_4)(HN)TiCH_3^+$ compared to −1.6 and 3.1 kcal/mol for $H_2Si(C_5H_4)(HN)TiC_2H_5^+$.

Comparing the energetic profiles for ethylene insertion at both of the presently considered contact ion pairs (Schemes 1 and 2), it is evident that formation of the intermediate π-complex and γ-agostic kinetic product are endothermic processes (∼6 and ∼8 kcal/mol relative to reactants) because of the unfavorable counteranion displacement from the Ti coordination sphere, and that these quantities are rather similar, thus indicating that the 10 kcal/mol energy shift observed in the naked cations on passing from $H_2Si(C_5H_4)(^tBuN)TiCH_3^+$ to $H_2Si(C_5H_4)(^tBuN)TiC_3H_7^+$ is absent. On the other hand, the overall energy barrier for ethylene insertion at $H_2Si(C_5H_4)(^tBuN)TiC_3H_7^+H_3CB(C_6F_5)_3^-$ (11.5 kcal/mol) is smaller than that associated with $H_2Si(C_5H_4)(^tBuN)TiCH_3^+\cdots H_3CB(C_6F_5)_3^-$ (15 kcal/mol for pathway B). This result suggests that initiation should be slower than propagation and that the differences are principally due to the greater reactivity of the $H_2Si(C_5H_4)(^tBuN)TiC_3H_7^+$ catalyst. In other words, the increased reactivity upon homologation of the Ti-bound alkyl moiety derives principally from the less electron-deficient nature of the metal center. This is borne out in experimental quenched-flow kinetic studies of initiation and propagation rates for the *rac*-C_2H_4(1-indenyl)$_2$-$ZrCH_3^+CH_3B(C_6F_5)_3^-$-catalyzed polymerization of 1-hexene.[18a] These studies demonstrate that initation is slower than propagation by a factor of 70 because of a substantial reduction in the transition state energy; $\Delta H^\ddagger = 11.5 \pm 1.5$ kcal/mol for the first 1-hexene insertion and $\Delta H^\ddagger = 6.4 \pm 1.5$ kcal/mol for subsequent insertions.

Comparing the present geometrical structures of the intermediate π-complex, transition state, and γ-agostic kinetic product with the ground state structure in $H_2Si(C_5H_4)(^tBuN)TiC_3H_7^+H_3CB(C_6F_5)_3^-$, the most striking aspect is the consistent $Ti^+\cdots[H_3CB(C_6F_5)_3]^-_{centr}$ elongation due to the displacement of the $H_3CB(C_6F_5)_3^-$ group by ethylene at the free coordination site of the metal center. The computed $Ti\cdots[H_3CB(C_6F_5)_3]_{centr}$ distances are similar to those obtained for stationary points of ethylene insertion at $H_2Si(C_5H_4)(^tBuN)$-$TiCH_3^+H_3CB(C_6F_5)_3^-$ along pathways B and C (π-complex, 7.36 vs 7.38 Å; transition state, 7.37 vs 7.08 Å; γ-agostic product, 6.85 vs 7.22 Å; Table 7 and Figures 6 and S1), thus indicating that the cation−anion interaction along the reaction coordinate for ethylene insertion at both $[H_2Si(C_5H_4)(^tBuN)]Ti(CH_3)^+H_3CB$-$(C_6F_5)_3^-$ (pathways B and C) and $[H_2Si(C_5H_4)(^tBuN)]Ti$-$(n$-$C_3H_7)^+H_3CB(C_6F_5)_3^-$ is similar. This result is in agreement with previous data on complete heterolytic ion pair dissociation for $H_2Si(C_5H_4)(^tBuN)TiR^+H_3CB$-$(C_6F_5)_3^-$ (R = CH_3 and C_3H_7), which indicate that the ΔH_{ips} value decreases upon further homologation of the alkyl chain (78 vs 74 kcal/mol), mainly because the *n*-propyl group participates in strong γ-agostic interactions that are more stabilizing than the α-agostic interactions available for methyl derivatives.[23b] The greater steric encumberance of the longer chain in the presently considered pathway is of minor relevance since it occupies a region far from the approaching ethylene and the counteranion.

Discussion

The present ab initio and B3LYP results demonstrate, in concurrence with growing experimental information, that any realistic description of CGC-mediated olefin polymerization must go beyond simple models because the active catalytic species are far more complex. The "actual" catalyst consists of *strongly interacting anion−cation pairs immersed in a solvation medium*. Theoretical analyses must go beyond the "naked cation" approach and explicitly evaluate the energetics of contact ion pair structure, solvation, and nonbonded interactions arising from the bulky perfluoroarylmetalate cocatalysts.

Energetics of Olefin Approach/Enchainment Trajectories. Analysis of the energetics associated with the three ethylene activation/insertion pathways at the $[H_2Si(C_5H_4)(^tBuN)]TiCH_3^+H_3CB(C_6F_5)_3^-$ ion pair reveals that the channel involving olefin approach distal to $H_3CB(C_6F_5)_3^-$ (pathway A) is energetically slightly favored and occurs via a concerted mechanism with no apparent intermediate. The other two channels (pathways B and C) involve the more congested space volume occupied by the $H_3CB(C_6F_5)_3^-$ group, are energetically and structurally similar, and proceed through two-step processes: (i) anion displacement with formation of an intermediate olefin π-complex; (ii) olefin insertion into the Ti−C bond (the slow step). These pathways are

energetically somewhat less favorable than A because they require greater ion pair separations. However, solvation may sufficiently stabilize charge-separated transition state structures to render these alternatives competitive in polar media. This would provide a pathway for ethylene insertion on either side of the catalyst, consistent with a "flip-flop"/"back-skipping" enchainment process.[1,8b] Pathways B and C exhibit the greatest similarities to ethylene insertion at the naked $H_2Si(C_5H_4)(^tBuN)TiCH_3^+$ cation,[23a] although the ion pair π-complexes and transition states lie substantially higher in energy due to the required counteranion displacement.

Analysis of the ethylene insertion process along reaction channels similar to pathways B and C at $[H_2Si(C_5H_4)(^tBuN)]TiC_3H_7^+H_3CB(C_6F_5)_3^-$ reveals marked similarities to insertion at Ti-methyl ion pairs in structures and energetics at all stationary points from the intermediate π-complexes to the γ-agostic kinetic product. However, the insertive transition state for $[H_2Si(C_5H_4)(^tBuN)]TiC_3H_7^+H_3CB(C_6F_5)_3^-$ is located lower in energy than that for the corresponding methyl complex (11.5 vs 15 kcal/mol). A similar energetic barrier reduction (4 kcal/mol) for the π-complex → transition state reaction coordinate has been also computed for the naked cation transformation $H_2Si(C_5H_4)(^tBuN)]TiCH_3^+ \rightarrow [H_2Si(C_5H_4)(^tBuN)]TiC_3H_7^+$. This feature together with (i) similar $Ti\cdots[H_3CB(C_6F_5)_3]_{centr}$ displacements in stationary points for both of the presently considered ion pairs and (ii) similar spatial dispositions of the *n*-propyl chain in stationary points along the reaction coordinates of $H_2Si(C_5H_4)(^tBuN)]TiC_3H_7^+$ and $[H_2Si(C_5H_4)(^tBuN)]TiC_3H_7^+H_3CB(C_6F_5)_3^-$, suggest that the energy barrier reduction for $Ti-C_3H_7^+$ insertion mainly depends on the metal center and its electron-deficient nature rather than the steric bulk of the *n*-propyl chain or the ion pairing strength.

Experimental energetic profiles for initial olefin coordination/insertion at a homogeneous single-site catalyst have been recently characterized via dynamic NMR studies of $[(CH_3)_2Si((CH_3)_4C_5)(^tBuN)]Zr^+X^-$, $(CH_3C_5H_4)_2Zr^+X^-$, and $(CH_3)_2Si(C_5H_4)_2Zr^+X^-$ betaines where $X^- = (\mu\text{-}C_4H_6)B(C_6F_5)_3^-$.[10] These systems afford estimates of $\Delta G^‡$ values associated with π-complex formation and subsequent insertion. In excellent agreement with the present results, it was shown that in all cases the transition state for olefin insertion into the Zr−C bond represents the highest point on the energy surface of the overall reaction sequence, i.e., olefin coordination occurs in a preequilibrium step, followed by rate-determining insertion.[10] The $[(CH_3)_2Si((CH_3)_4C_5)(^tBuN)]Zr^+X^-$ catalyst exhibits much lower polymerization activity than the other systems analyzed, and $\Delta G^‡$ values for propylene coordination and insertion, relative to the free reagents in toluene, are 16.4 and 18.8 kcal/mol, respectively. Although there are admittedly differences from the systems studied here computationally, a qualitative analysis can be attempted. Ethylene coordination and insertion energy barriers (**TS-I** and **TS-II**, respectively) along pathway B (9 and 10 kcal/mol; Table 1) are lower than experiment for $[(CH_3)_2Si((CH_3)_4)C_5(^tBuN)]Zr^+X^-$ (16.4 and 18.8 kcal/mol).[10b] The difference doubtless reflects the absence of entropic, thermal, and zero-point corrections to the computed free energy. Including these terms for insertion transition state **TS-II** yields $\Delta G°_{298} = 22$ kcal/mol, in reasonable agreement with the experimental value of 18.8 kcal/mol.[10b]

The kinetic *n*-propyl product of pathway A has a metastable conformation that can readily rearrange to a manifold of more stable, nearly degenerate, geometries having short $Ti^+\cdots[H_3CB(C_6F_5)_3]^-_{centr}$ contacts. These conformers do not exhibit significant *n*-propyl chain agostic interactions due to the electron density transfer from the coordinated borate counteranion. The kinetic products formed along routes B and C closely resemble those formed with the parent naked cations since the counteranion remains outside the Ti coordination sphere. Thus, the Ti-propyl chain is involved in an γ-agostic interaction which can rearrange to β-agostic products, similar to the naked cation *n*-propyl product. These conformers can then rearrange to ground state geometries similar to those from pathway A (Figures 8 and 9; **2**−**7**). Moreover, γ- or β-agostic structures **8**−**10** may be stabilized by solvation due to the greater ion pair separation and accompanying degrees of freedom (entropic contributions). The structural nature of these Ti-alkyl conformations, their mobility, and the modulation of these characteristics by ion pairing with the cocatalyst strongly support experimental postulates of how direct and indirect effects control syndiospecific and isospecific enchainment processes for propylene.[1,8b]

Associative versus Dissociative Insertion Processes. Two alternative ion pair reorganization mechanisms, either associative or dissociative, can be associated with ethylene insertion, depending on the relative stabilities of the *n*-propyl conformers.[26b,27] An associative mechanism is expected for closely ion-paired conformers having short $Ti^+\cdots H_3CB(C_6F_5)_3^-$ contacts, hence having considerably higher stability than "separated" ion pairs. In this case, the chain "back-skips" on each insertion, and the counteranion recombines with the catalyst cation after insertion, to form a new contact ion pair. Rapid site epimerization[1,8b,13] between the two "open" metal coordination sites is restricted by the ion pair tightness, and for propylene polymerization, either atactic or isotactic polypropylene can, in principle, be obtained.[3a] In contrast, a dissociative mechanism requires that the stabilities of "separated ion pair" structures **8**−**10** (Figures 6 and S2) are comparable to or greater than those of structures having short $Ti^+\cdots CH_3B(C_6F_5)_3^-$ contacts (as in the present case). The growing chain can now migrate between two open metal sites ("flip-flop" mechanism) with olefin insertion alternating between the two sides of the catalyst. In this case, syndiotactic polypropylene would be obtained from a C_s-symmetric catalyst. For these reasons associative and dissociative mechanisms have been also referred to as chain nonmigratory (or stationary) insertion and migratory insertion mechanisms, respectively (eqs 1 and 2).[3,27] The present analysis can be used to understand experimental tacticity data for propylene polymerization at CGC-based catalysts.[5b−d] Thus, both C_s-symmetric $[(CH_3)_2Si(fluorenyl)(^tBuN)]TiCl_2$ and $[(CH_3)_2Si((CH_3)_4C_5)](^tBuN)]TiCl_2$ precatalysts, activated by MAO, afford syndiotactic-rich polypropylene, suggesting two symmetry-related active polymerization sites at the same metal center (arguing for the dissociative mechanism).[5b−d]

Chain stationary insertion

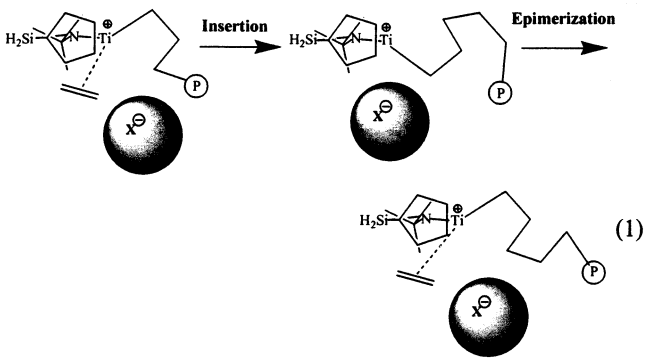

(1)

Chain migratory insertion

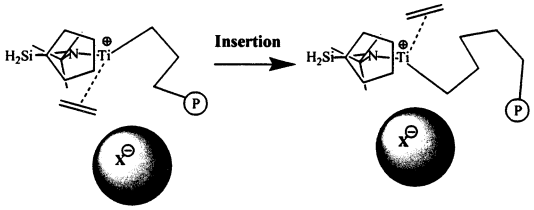

(2)

In recent work involving C_s-symmetric $[Me_2C(Cp)$-(fluorenyl)$]ZrR^+X^-$ (X^- = counteranions of varying coordinating tendency)-mediated syndiotactic propylene polymerization in nonpolar solvents, X^--dependent polymerization rate and stereoerror patterns arising from site epimerization/flip-flop/backskip processes could be directly correlated with the strength of the ion pairing.[8b] Moreover, in polar solvents, the great X^--dependent dispersion in propagation rates and enchainment stereospecificity almost vanishes, clearly indicating the importance of ion pairing and solvation in the enchainment process. Another example is a series of $(CH_3)_2Si$-[(fluorenyl)(^{t}BuN)]$ZrCl_2$-based catalysts[5f] where inversion of stereoselectivity, from syndiospecific to isospecific, is reported upon changing cocatalyst. The ion pair remains largely dissociated with MAO, and the growing chain can migrate between two equatorial Zr coordination sites (a dissociative mechanism). However, more strongly coordinating $B(C_6F_5)_4^-$ apparently does not allow ready migration, leaving only one predominant site available for olefin insertion (associative mechanism).[5e,f]

d^0 Olefin Complex Structures and Dynamics. The present results are also useful in understanding the structures and dynamic properties of the cationic d^0 π-complexes $[(CH_3)_2Si(R_4C_5)(^t$BuN)]Ti[OC$(CH_3)_2$-$CH_2CH_2CH{=}CH_2]^+A^-$ (**II**),$[R_5C_5]_2Zr[OC(CH_3)_2CH_2CH_2CH{=}$-$CH_2]^+A^-$, $[R_5C_5]_2ZrCH_2CH_2C(CH_3)_2CH{=}CH_2{}^+A^-$ ($A^- = H_3CB(C_6F_5)_3^-$, $B(C_6F_5)_4^-$), and $[(CH_3)_5C_5]_2YCH_2CH_2C$-$(CH_3)_2CH{=}CH_2$.[11] Thus, olefin facial interchange in $[(CH_3)_2Si(R_4C_5)(^t$BuN)]Ti[OC$(CH_3)_2CH_2CH_2CH{=}$-$CH_2]^+A^-$ complexes does not occur through an associative mechanism involving displacement of the olefin by the anion, but rather involves rate-limiting dissociation of the olefin accompanied by fast inversion at the metal center without direct anion involvement.[11a] These data again highlight the competition revealed in the present computational work between olefin and counteranion to saturate the CGC-Ti coordination sphere. Moreover, olefin C_{int} and C_{term} NMR chemical shift dispersions are

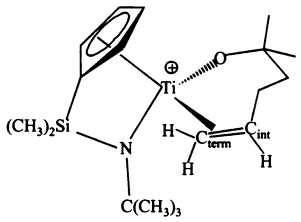

II

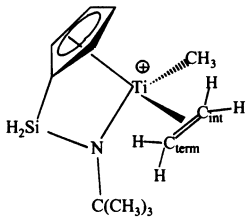

III

consistent with unsymmetrical Ti-olefin bonding in $[(CH_3)_2Si(R_4C_5)(^t$BuN)]Ti[OC$(CH_3)_2CH_2CH_2CH{=}CH_2]^+A^-$ complexes since it involves a weak Ti$-C_{term}$ and minimal Ti$-C_{int}$ interaction. This, in turn, induces polarization of the C=C π bond with positive charge buildup at C_{int} (**IV**).[11a] Similar shift patterns are observed in the

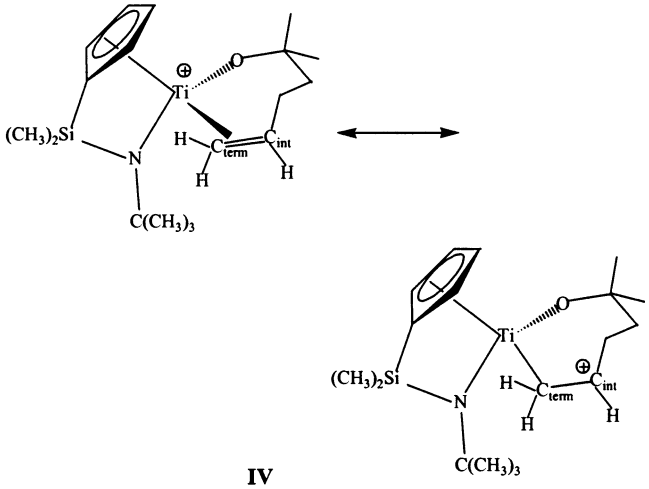

IV

ground states of all the aforementioned metallocenium π-complexes.[11] In the case of $(C_5H_5)_2Zr[OC(CH_3)_2$-$CH_2CH_2CH{=}CH_2]^+A^-$ complexes, X-ray data indicate very different Zr$-C_{int}$ and Zr$-C_{term}$ contacts (2.89(2) and 2.68(2) Å, respectively).[11b]

The present computed metrical data for the $[H_2Si$-$(C_5H_4)(^t$BuN)]$TiCH_3(C_2H_4)^+\cdots H_3CB(C_6F_5)_3^-$ π-complex (**III**) similarly indicate unsymmetrical ethylene coordination (Figures 6 and S1; Table 2). In this case, however, one Ti$\cdots C_{term}$ (C12) contact is longer (Ti$-$C(12) $\approx$ 2.9 Å) than the other Ti$-C_{term}$ (Ti$-$C(13) $\approx$ 2.6 Å; labeling refers to that of Jordan et al.[11a]). The present, reversed Ti$-C_{int}$ and Ti$-C_{term}$ distances imply inverted polarization of the olefinic C atoms (Mulliken charges on H_2C_{term} and H_2C_{int} are +0.23 and +0.05 eu, respectively) with respect to that suggested by the NMR data. This is likely a consequence of the σ-bonded resonance contribution which allows delocalization of the positive charge from Ti to the vinyl carbon. In $[(CH_3)_2Si(R_4C_5)(^t$BuN)]-Ti[OC$-(CH_3)_2CH_2CH_2CH{=}CH_2]^+A^-$ complexes, the Markovnikov rule favors localization of positive charge

on C_{int} (secondary carbon) relative to C_{term} (primary carbon). In the present systems, a positive charge is located on both ethylene C atoms, and therefore, the stronger Ti−C_{int} interaction is driven by interligand steric repulsion (**V**). The present conclusions also agree

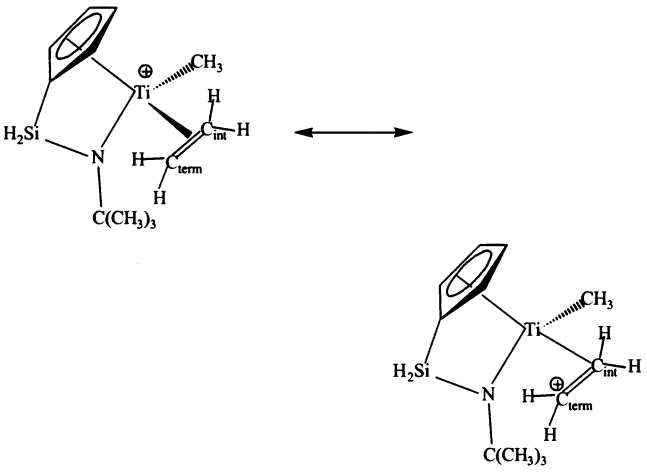

V

well with the model of Morokuma et al.[16h] for ethylene and propylene coordination in $Cl_2TiCH_3^+$ π-complexes. Here ground state structures having the strongest interactions between either Ti−C_{int} or Ti−C_{term} depend on the nature of the olefin. For the ethylene π-complex, the Ti−C_{int} interaction is stronger than Ti−C_{term}, while for propylene, the Ti−C_{term} interaction is stronger than Ti−C_{int} (**VI** vs**VII**). This interpretation agrees with

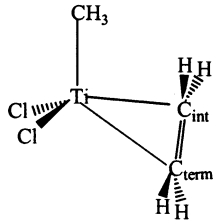

VI

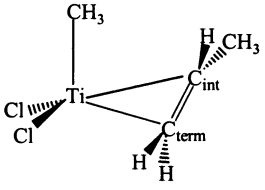

VII

calculated structures of propylene π-complexes in variously substituted $H_2Si(C_5R_4(^tBuN)TiR{\cdot}(C_3H_6)^+$ catalysts. Depending on the propylene-CH_3 position, alternating stronger Ti···C_{int} or Ti···C_{term} interactions are observed and, hence, alternating shorter or longer bond distances.[34]

Comparisons with Previous DFT Studies. The present findings are in general agreement with static density functional and first-principles molecular dynamic results reported for ethylene insertion into the Zr−ethyl functionality of $(C_5H_5)_2ZrC_2H_5^+H_3CB(C_6F_5)_3^-$ reported by Ziegler et al.[26] They report that the $(C_5H_5)_2ZrC_2H_5^+H_3CB(C_6F_5)_3^-$ ground state geometry does not contain Zr−ethyl agostic interactions but that there exist structures close in energy having short Zr···$H_3CB(C_6F_5)_3^-$ contacts and strong β-agostic interactions. In contrast, similar structures are not detected in the present $[H_2Si(C_5H_4)(^tBuN)]TiC_3H_7^+H_3CB(C_6F_5)_3^-$ calculations because the closely associated counteranion precludes agostic interactions with the *n*-propyl chain. We detect strong β- or γ-agostic interactions only when the counteranion is far removed from the metal coordination sphere. These differences probably reflect the established greater tendency of DFT methodologies to overestimate agostic interactions, as previously shown for metallocenes and CGC naked cations.[16f,23a] The present results, however, find a basis in chemical intuition since cation−anion interactions as operative in $[H_2Si(C_5H_4)(^tBuN)]TiC_3H_7^+H_3CB(C_6F_5)_3^-$ are doubtless stronger than the cation−dipole interactions of agostic structures. While the crystal structure of $(C_5H_4CH_3)_2ZrC_2H_5[P(CH_3)_3]^+B(C_6H_5)_4^-$ exhibits a β-agostic interaction in the presence of a coordinated $P(CH_3)_3$ molecule,[33] note that the steric demands and complexation properties of $B(C_6H_5)_4^-$ are likely to be very different from those of $H_3CB(C_6F_5)_3^-$, rendering comparisons difficult.

The ethylene insertion pathway into the Zr−ethyl bond of the $(C_5H_5)_2ZrC_2H_5^+H_3CB(C_6F_5)_3^-$ contact ion pair distal to the $H_3CB(C_6F_5)_3^-$ group (present pathway A) was also investigated by Ziegler et al.[26b] The computed energy profile does not show an intermediate, and the barrier in toluene is reported to be 11.6 kcal/mol, in agreement with the present ab initio result for pathway A in benzene of 8 kcal/mol. In the $(C_5H_2)_2$-$ZrC_2H_5^+H_3CB(C_6F_5)_3^-$ study, no quantitative analysis was reported for alternative enchainment pathways, analogous to the present pathways B and C; however, these authors provide estimates for similar insertion channel barriers, namely, ∼9 kcal/mol for the formation of olefin-separated ion pairs from the contact ion pairs and 5−7 kcal/mol for ethylene insertion. These data are reasonably similar to the π-complex formation (2 kcal/mol) and insertion barrier (8 kcal/mol) presently found for pathways B and C. Note, however, that Ziegler et al.[26b] suggest that olefin complexation may constitute the greatest barrier in the insertion process, with subsequent insertion proceeding without an apparent barrier. In contrast, both the present ab initio and experimental[10] results show that in all cases examined the transition state for olefin insertion into the M−C bond represents the energetically highest point on the energy surface for the olefin activation/enchainment process. It is possible that the tendency of DFT approaches to underestimate insertion barriers in this class of reactions[23a] is the explanation for these discrepancies. In agreement with the present results, analysis of post-insertion counteranion mobility in the $(C_5H_5)_2$-$Zr(n\text{-}C_4H_9)^+H_3CB(C_6F_5)_3^-$ contact ion pair by these authors[26b] suggests that both dissociative and associative mechanisms may be operative and that the prevalence of any single pathway is sensitive to specifics of the polymerization process.

Nifant'ev et al.[25] also reported a DFT theoretical investigation of ethylene insertion into the Zr−ethyl

(34) Motta, A.; Lanza, G.; Fragalà, I. L.; Marks, T. J. Manuscript in preparation.

of the $(C_5H_5)_2ZrC_2H_5^+H_3CB(C_6F_5)_3^-$ and $(C_5H_5)_2ZrC_2H_5^+B(C_6F_5)_4^-$ contact ion pairs, explicitly including the entropic contribution but ignoring solvation effects and metal relativistic effects. They mainly focused on a reaction channel similar to pathway C and, in agreement with present results, found that an energy barrier of $\Delta H^{\ddagger} = 10$ kcal/mol for the anion displacement is required for formation of the $(C_5H_5)_2ZrC_2H_5(C_2H_4)^+H_3CB(C_6F_5)_3^-$ intermediate π-ethylene complex. The stability of the intermediate and of the final product are comparable to those presently obtained (1 and −33 kcal/mol vs 6 and −24 kcal/mol). In agreement with the present data, the geometries of the insertive transition states are characterized by large Zr···B elongations (1.1−1.2 Å). However, the insertion barrier (2 kcal/mol) is considerably lower than that found in this work.

Conclusions

The first analysis of combined counteranion, solvation, and entropic effects on the structural energetics of ethylene activation and enchainment at the Ti−methyl bond of a constrained geometry catalyst−cocatalyst ion pair has been carried out at the proven ab initio MP2 level of theory employing a double-ζ basis set. Striking and instructive differences are detected with respect to the same processes in the corresponding naked organotitanium cation. Thus, in the presence of the counteranion, potential energy surfaces in all reaction pathways examined are shifted to substantially higher energies because of the large required counteranion displacements. The initial cation−anion separation along all reaction channels is followed by formation of an insertive four-membered metallacylic transition state which is found to be rate-limiting, in excellent agreement with experiment. The transition state energies strongly depend on the solvent polarity because it partially diminishes cation−anion attractions, implying strong attenuation of ion pairing effects on catalytic activity and selectivity as solvent polarity increases, in general agreement with experiment.[2e,8b,14c] Reaction channels that involve olefin approach proximal to the counteranion result in formation of stable olefin π-complexes prior to insertion. Structural analysis of the $[H_2Si(C_5H_4)(^tBuN)]Ti(n\text{-}C_3H_7)^+H_3CB(C_6F_5)_3^-$ ion pair reveals the presence of several minima on the energy hypersurface which can be classified according to how the metal center Lewis acidity is quenched: (i) by the counteranion through CH_3 group or aryl F atom coordination, or (ii) by intramolecular agostic interactions. In the latter conformers, characterized by long $Ti^+\cdots[H_3CB(C_6F_5)_3^-]_{centr}$ contacts, the alkyl chain screens the counteranion and assumes spatial arrangments similar to those found in the Ti *n*-propyl naked cation. The relative stabilities of these two types of structures depend on solvent dielectric constant and entropic contributions, and their populations underscore the appreciable flexibility of the almost exclusively electrostatic $[H_2Si(C_5H_4)(^tBuN)]Ti(n\text{-}C_3H_7)^+\cdots H_3CB(C_6F_5)_3^-$ linkage (in excellent agreement with experiment[13]) and is the first theoretical evidence for the existence of stable structures with strong metal−alkyl β- or γ-agostic interactions, similar to those found in the corresponding naked cations, even in the presence of a tightly paired counteranion, a nearly ubiquitous component of single-site olefin polymerization catalysis.[1]

The higher barrier found here for the rate-determining ethylene insertion at $[H_2Si(C_5H_4)(^tBuN)]TiCH_3^+H_3CB(C_6F_5)_3^-$ compared with that found at $[H_2Si(C_5H_4)(^tBuN)]Ti(n\text{-}C_3H_7)^+H_3CB(C_6F_5)_3^-$ is interestingly in agreement with the recent experimental finding that polymer chain initiation reaction is ∼70× slower than propagation for the *rac*-$C_2H_4(1\text{-indenyl})_2ZrCH_3^+CH_3B(C_6F_5)_3^-$-catalyzed polymerization of 1-hexene[18a] because of a substantial reduction in the insertive transition state energy. As far as methodological approaches are concerned, comparative analyses of geometries obtained at HF and B3LYP show little variation in metrical parameters, thus indicating that correlation effects do not produce drastic changes for systems with weak bonding interactions such as those presently considered. Energetics derived at the HF/MP2 level are similar to those derived at the B3LYP/B3LYP. However, small variations in transition state stabilities have also been observed.

Acknowledgment. This research was supported by the Ministero dell'Università e della Ricerca Scientifica e Tecnologica (MURST Rome), the Consiglio Nazionale delle Ricerche (Rome), and the U.S. Department of Energy (grant 86ER13511). We thank Mr. T. Jensen for expert assistance with the graphics.

Supporting Information Available: Figures S1 and S2 and a complete list of Cartesian coordinates of all structures presently analyzed. This material is available free of charge via the Internet at http://pubs.acs.org.

OM0207764